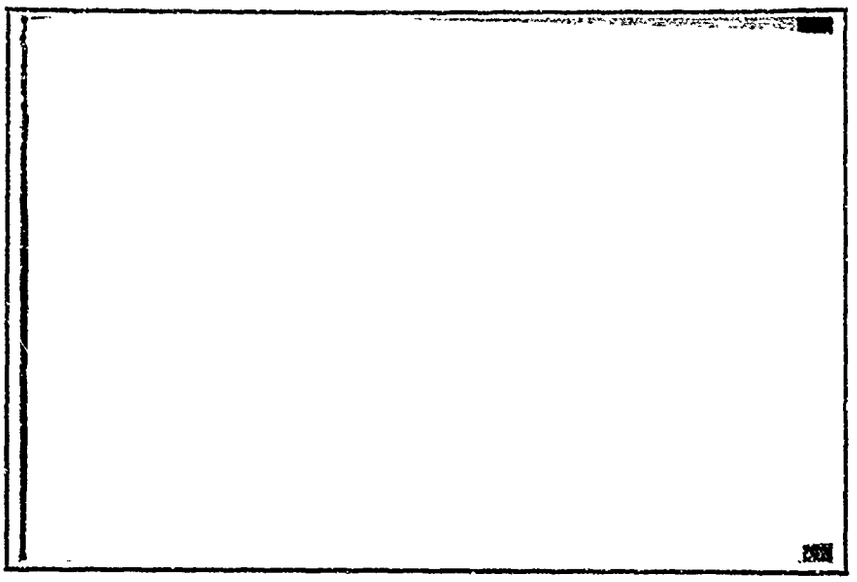

הטכניון – מכון טכנולוגי לישראל
המקולטה להנדסת אווירונוטית

TECHNION – ISRAEL INSTITUTE OF TECHNOLOGY

DEPARTMENT OF AERONAUTICAL ENGINEERING

HAIFA, ISRAEL

F 61052-70-C-0005

FSR - II

FEBRUARY 1971

FINAL SCIENTIFIC REPORT - PART II

CALIBRATION OF THE TAILORED INTERFACE 8" x 10" SHOCK TUNNEL

by

A. KURITZKY AND J. ROM
Department of Aeronautical Engineering
Technion - Israel Institute of Technology,
Haifa, Israel.

T.A.E. REPORT No. 116

The research reported in this paper has been sponsored in part by the Aerospace Research Laboratories, under Contract F 61052-70-C-0005, through the European Office of Aerospace Research (OAR) United States Air Force. This research is part of the separated flow research program of the ARL, Thermomechanics division.

UNCLASSIFIED

Security Classification

DOCUMENT CONTROL DATA - R&D

(Security classification of title, body of abstract and indexing annotation must be entered when the overall report is classified)

1 ORIGINATING ACTIVITY (Corporate author) TECHNION RESEARCH AND DEVELOPMENT FOUNDATION AERONAUTICAL ENGINEERING LABORATORY, HAIFA, ISRAEL.	2a REPORT SECURITY CLASSIFICATION Unclassified 2b GROUP

3 REPORT TITLE

CALIBRATION OF THE TAILORED INTERFACE 8" x 10" SHOCK TUNNEL

4 DESCRIPTIVE NOTES (Type of report and inclusive dates)

FINAL REPORT

5 AUTHOR(S) (Last name, first name, initial)

A. KURITZKY
J. ROM

6 REPORT DATE	7a TOTAL NO OF PAGES	7b. NO. OF REFS
JANUARY 1971	50	21

8a CONTRACT OR GRANT NO. F61052-70-C-0005 b PROJECT NO 7063 c 61102F d 681307	9a ORIGINATOR'S REPORT NUMBER(S) T.A.E. REPORT No. 116 9b OTHER REPORT NO(S) (Any other numbers that may be assigned this report)

10 AVAILABILITY/LIMITATION NOTICES

This document has been approved for public release and sale; its distribution is unlimited.

11 SUPPLEMENTARY NOTES	12 SPONSORING MILITARY ACTIVITY
	AEROSPACE RESEARCH LABORATORIES (ARN) WRIGHT-PATTERSON, AFB, OHIO, 45433

13 ABSTRACT

This work presents the design considerations and the calibration of a shock tunnel for aerodynamic measurements at hypersonic Mach numbers. The shock tunnel is composed of a shock tube which is used for the production of high temperature and high pressure air reservoir, which is then expanded through a supersonic nozzle, thereby attaining high Mach number flow in the test section.

In order to obtain maximum test time the "tailored" mode of operation is used for this shock tunnel. A method for calculating the optimum ratio of the compression chamber length to the low pressure tube length for a given total shock tube length that will result in a maximum test duration is presented. Shock tube experimental results at "tailored" condition for hydrogen (driver gas) and air (as the driven gas), both at room temperature, indicate that by proper design a reservoir of air with an enthalpy of 2000 Btu/lb. can be produced for a duration of more than 2.0 msec. for a total shock tube length of 9 meters.

The flow in the test section is calibrated using a total pressure rake and by static pressure measurements and measurements of stagnation point heat transfer rates at various points in the test section. The flow conditions are then calculated using the theoretical relations for stagnation point heat transfer rates. The shock tunnel test section has been thus calibrated at two nozzle positions: one $A/A^* = 250$ resulting in a nominal Mach number of 5.5 and $A/A^* = 500$ resulting in a nominal Mach number of 7.

The experimental results show a reasonably uniform flow in the horizontal plane with a relatively thin boundary layer. While in the vertical plane only a central core of about half test section height has uniform flow conditions and is suitable for aerodynamic testing.

DD FORM 1 JAN 64 1473

Unclassified

Security Classification

ABSTRACT

This work presents the design considerations and the calibration of a shock tunnel for aerodynamic measurements at hypersonic Mach numbers. The shock tunnel is composed of a shock tube which is used for the production of high temperature and high pressure air reservoir, which is then expanded through a supersonic nozzle,thereby attaining high Mach number flow in the test section.

In order to obtain maximum test time the "tailored" mode of operation is used for this shock tunnel. A method for calculating the optimum ratio of the compression chamber length to the low pressure tube length for a given total shock tube length that will result in a maximum test duration is presented. Shock tube experimental results at "tailored" condition for hydrogen (driver gas) and air (as the driven gas), both at room temperature, indicate that by proper design a reservoir of air with an enthalpy of 2000 Btu/lb. can be produced for a duration of more than 2.0 msec. for a total shock tube length of 9 meters.

The flow in the test section is calibrated using a total pressure rake and by static pressure measurements and measurements of stagnation point heat transfer rates at various points in the test section. The flow conditions are then calculated using the theoretical relations for stagnation point heat transfer rates. The shock tunnel test section has been thus calibrated at two nozzle positions: one $A/A^* = 250$ resulting in a nominal Mach number of 5.5 and $A/A^* = 500$ resulting in a nominal Mach number of 7.

14 KEY WORDS	LINK A		LINK B		LINK C	
	ROLE	WT	ROLE	WT	ROLE	WT
1. Tailored Shock Tunnel 2. Calibration of the Shock Tunnel						

INSTRUCTIONS

1. ORIGINATING ACTIVITY: Enter the name and address of the contractor, subcontractor, grantee, Department of Defense activity or other organization *(corporate author)* issuing the report.

2a. REPORT SECURITY CLASSIFICATION: Enter the overall security classification of the report. Indicate whether "Restricted Data" is included. Marking is to be in accordance with appropriate security regulations.

2b. GROUP: Automatic downgrading is specified in DoD Directive 5200.10 and Armed Forces Industrial Manual. Enter the group number. Also, when applicable, show that optional markings have been used for Group 3 and Group 4 as authorized.

3. REPORT TITLE: Enter the complete report title in all capital letters. Titles in all cases should be unclassified. If a meaningful title cannot be selected without classification, show title classification in all capitals in parenthesis immediately following the title.

4. DESCRIPTIVE NOTES: If appropriate, enter the type of report, e.g., interim, progress, summary, annual, or final. Give the inclusive dates when a specific reporting period is covered.

5. AUTHOR(S) Enter the name(s) of author(s) as shown on or in the report. Enter last name, first name, middle initial. If military, show rank and branch of service. The name of the principal author is an absolute minimum requirement.

6. REPORT DATE: Enter the date of the report as day, month, year, or month, year. If more than one date appears on the report, use date of publication.

7a. TOTAL NUMBER OF PAGES: The total page count should follow normal pagination procedures, i.e., enter the number of pages containing information.

7b. NUMBER OF REFERENCES: Enter the total number of references cited in the report.

8a. CONTRACT OR GRANT NUMBER: If appropriate, enter the applicable number of the contract or grant under which the report was written.

8b, 8c, & 8d. PROJECT NUMBER: Enter the appropriate military department identification, such as project number, subproject number, system numbers, task number, etc.

9a. ORIGINATOR'S REPORT NUMBER(S): Enter the official report number by which the document will be identified and controlled by the originating activity. This number must be unique to this report.

9b. OTHER REPORT NUMBER(S): If the report has been assigned any other report numbers *(either by the originator or by the sponsor)*, also enter this number(s).

10. AVAILABILITY/LIMITATION NOTICES: Enter any limitations on further dissemination of the report, other than those imposed by security classification, using standard statements such as:

(1) "Qualified requesters may obtain copies of this report from DDC."

(2) "Foreign announcement and dissemination of this report by DDC is not authorized."

(3) "U. S. Government agencies may obtain copies of this report directly from DDC. Other qualified DDC users shall request through _____."

(4) "U. S. military agencies may obtain copies of this report directly from DDC. Other qualified users shall request through _____."

(5) "All distribution of this report is controlled. Qualified DDC users shall request through _____."

If the report has been furnished to the Office of Technical Services, Department of Commerce, for sale to the public, indicate this fact and enter the price, if known.

11. SUPPLEMENTARY NOTES: Use for additional explanatory notes.

12. SPONSORING MILITARY ACTIVITY: Enter the name of the departmental project office or laboratory sponsoring *(paying for)* the research and development. Include address.

13. ABSTRACT: Enter an abstract giving a brief and factual summary of the document indicative of the report, even though it may also appear elsewhere in the body of the technical report. If additional space is required, a continuation sheet shall be attached.

It is highly desirable that the abstract of classified reports be unclassified. Each paragraph of the abstract shall end with an indication of the military security classification of the information in the paragraph, represented as *(TS), (S), (C), or (U)*.

There is no limitation on the length of the abstract. However, the suggested length is from 150 to 225 words.

14. KEY WORDS: Key words are technically meaningful terms or short phrases that characterize a report and may be used as index entries for cataloging the report. Key words must be selected so that no security classification is required. Identifiers, such as equipment model designation, trade name, military project code name, geographic location, may be used as key words but will be followed by an indication of technical context. The assignment of links, rules, and weights is optional.

The experimental results show a reasonably uniform flow in the horizontal plane with a relatively thin boundary layer. While, in the vertical plane only a central core of about half test section height has uniform flow conditions and is suitable for aerodynamic testing.

TABLE OF CONTENTS

	PAGE No.
ABSTRACT	I - II
LIST OF SYMBOLS	V - VI
LIST OF FIGURES	VII - IX
I. INTRODUCTION	1
II. CALCULATION OF THE TAILORED SHOCK TUBE CHARACTERISTICS	2
2.1. Calculation of Tailoring Conditions	2 - 5
2.2. Calculation of the Duration of Flow at Tailored Conditions	6 - 7
2.3. Calculation of Optimum "Tailored" Shock Tube Design	8 - 9
2.4. The Additional Reservoir Pressure	10 - 13
III. FLOW IN THE HYPERSONIC SHOCK TUNNEL NOZZLE	14
3.1 Calculation of the Stagnation Conditions (Conditions in Region 5)	14 - 16
3.2. The Starting Process in the Shock Tunnel Nozzle	17 - 18
3.3. The Calculation of the Stagnation Point Heat Transfer in the Hypersonic Shock Tunnel Flow	18 - 20
IV. THE EXPERIMENTAL SYSTEM	21
4.1. The Shock Tunnel	21 - 23
4.2. The Instrumentation System	23 - 27
V. EXPERIMENTAL RESULTS	28
5.1. Experimental Results in the Shock Tube	28 - 31
5.2. Experimental Results in the Shock Tunnel	31 - 34
VI. SUMMARY AND CONCLUSIONS	35 - 36

TABLE OF CONTENTS (CONT'D)

	PAGE No.
APPENDIX A - Calculation of the Velocity Gradient at the Stagnation Point of a Sphere in Hypersonic Flow	37 - 39
REFERENCES	40 - 41

LIST OF SYMBOLS

A	- cross-sectional area
A^*	- cross-sectional area at the throat
C_p	- specific heat at constant pressure
D	- diffusion coefficient
I	- electric current
L	- $\frac{\rho D_p}{k}$ - Lewis number
M	- Mach number
M_s	- incident shock Mach number
M_{s_2}	- reflected shock Mach number
M_{s_T}	- incident shock Mach number at tailoring conditions
Pr	- Prandtl number
p	- pressure
R	- electrical resistance, gas constant
Re	Reynolds numbers
T	- temperature
U	- velocity
V	- electric voltage
Z	- compressibility
a	- sonic velocity
g	- acceleration of gravity
h	- enthalpy
k	- conductivity
q	- heat transfer rate

r_o - heat transfer gauge diameter.

t - time

α - thermal expansion coefficient, degree of atomic dissociation

γ - specific heat ratio

δ - area ratio between the driven gas region and the nozzle throat in the driver gas region

ρ - density

μ - viscosity coefficient

SUBSCRIPTS

c.s. - contact surface

e - flow outside of the boundary layer

t - total

T - throat

w - wall

LIST OF FIGURES

FIGURE No.

1. Flow regions in a shock tube.
2. Hot flow duration, for unit length, in shock tube.
3. a_3/a_2 Vs M_s for air as a driven gas and different driver gases.
4. Calculated time events in the actual shock tube.
5. Calculated time events for maximum test duration shock tube.
6. Shock tube with a nozzle in the driver section.
7. p-u diagram for shock tube.
8. Chemical reactions in the shock heated air.
9. Flow chart for computing air properties in thermodynamic equilibrium flow.
10. Theoretical heat transfer rates Vs. flow Mach number (potential flow over a sphere).
10A. Theoretical heat transfer rate Vs. Mach number at the supersonic nozzle - (Newtonian pressure distribution approximation).
11. Main parts of the shock tunnel.
12. General view of the shock tunnel.
13. The supersonic nozzle
14. The measurement system.
15. Total pressures rake.
16. Stagnation heat transfer.

LIST OF FIGURES (CONT'D)

FIGURE No.

17. General view of the electronic equipment.

18. Incident shock wave attenuation along the shock tube.

19. Initial pressure ratio across the shock tube diaphragm for H_2/Air at room temperature.

20. Pressure ratio across incident shock wave.

21. Ratio of pressure behind the reflected shock wave to the initial pressure in the shock tube.

22. Traces of pressure measurement at the end of the shock tube.

23. Traces of pressure measurement at the end of the shock tube.

24. Ratio of equilibrium pressure at the end of the shock tube to the initial pressure in the shock tube.

25. The supersonic nozzle.

26. Pressure gauge traces at the test section.

27. Heat transfer rate measurements traces at the test section.

28. ΔV Vs. t from heat transfer rate measurement.

29. Total pressures behind the shock wave, horizontal distribution. Nozzle in position A.

30. Total pressure behind the shock wave, vertical distribution. Nozzle in position A.

31. Total pressures behind the shock wave, horizontal distribution. Nozzle in position B.

32. Total pressures behind the shock wave, vertical distribution. Nozzle in position B.

LIST OF FIGURES (CONT'D)

FIGURE No.

33. Vertical distribution of static pressures. Nozzle in position A.

34. Vertical distribution of static pressures. Nozzle in position B.

35. Horizontal distribution of stagnation point heat transfer rates. Nozzle in position A.

36. Vertical distribution of stagnation point heat transfer rates. Nozzle in position A.

37. Horizontal distribution of stagnation point heat transfer rates. Nozzle in position B.

38. Vertical distribution of stagnation point heat transfer rates. Nozzle in position B.

I. INTRODUCTION

The shock tunnel utilizes for its operation the reservoir of high temperature, high pressure air at the end of the shock tube. This air is then expanded through the hypersonic nozzle to high Mach numbers. The flow regions in the shock tube are shown in a schematic diagram in Figure 1. The hot gas enclosed between the first shock wave and the contact surface (region 2) may be utilized for aerodynamic measurements. The duration of this flow depends upon the shock Mach number and the length of the low pressure section. The time duration for a unit length of low pressure section as a function of the shock wave Mach number is presented in Figure 2. If now, a supersonic nozzle is connected to the end of the shock tube it is possible to accelerate the shock heated air in region 2 to a hypersonic Mach number. This arrangement of the "flow through" shock tunnel is limited by the very short test duration. As shown in Fig. 2, this time can be few hundreds of microseconds for a tunnel of acceptable length, furthermore, this test duration decreases with increasing initial shock Mach number. Another method of operating the shock tunnel utilizes the hot gas behind the reflected shock wave at the end of the shock tube at the conditions of "tailored interface". This condition is achieved when the shock wave which is reflected from the end of the shock tube encounters the contact surface without any reflected disturbances. At "tailored" conditions a much longer (few milliseconds) test time is available for shock tunnel applications.

II. CALCULATION OF THE TAILORED SHOCK TUBE CHARACTERISTICS

2.1. Calculation of Tailoring Conditions

The calculation of the tailored conditions is described in Ref. 3. A short review of this calculation is presented in order to facilitate the description of the present study

The conditions which must exist at the point of encounter between the reflected shock wave and the contact surface is that the static pressure and velocities must be equal on both sides of the contact surface i.e. (see Fig. 1).

$$U_6 = U_7$$

$$P_6 = P_7$$

The equation which relates the velocities and pressures on the two sides of a moving shock wave is

$$\frac{U_d - U_u}{a_u} = \delta(P_{du} - 1)(\alpha P_{du} + 1)^{-0.5} \qquad (1)$$

where:

u - upstream of the shock wave

d - downstream of the shock wave

and

$$\delta = \left[\frac{2}{\gamma(\gamma - 1)}\right]^{0.5}$$

$$\alpha = \frac{\gamma + 1}{\gamma - 1}$$

and the positive velocity direction is in the direction of movement of the shock wave. From these:

$$\frac{U_3 - U_7}{a_3} = \delta_4 (P_{73} - 1)(\alpha_4 P_{73} + 1)^{-0.5} \qquad (2)$$

Since $U_5 = 0$

$$\frac{U_6}{a_5} = \delta_1 (P_{65} - 1)(\alpha_1 P_{65} + 1) \qquad (3)$$

For the case in which the reflected disturbances are rarefaction waves we obtain:

$$\frac{U_6}{a_5} = - \frac{1}{\gamma_1 p_1} (1 - P_{65}^{\beta_1}) \qquad (4)$$

where:

$$\beta = \frac{\gamma - 1}{2\gamma}$$

Since $U_6 = 0$ is the contact surface velocity after the encounter, it follows from Eqs. 3 and 4 that the contact surface moves toward the nozzle when the reflected disturbances are shock waves and away from the nozzle when the reflected disturbances are rarefaction waves.

From the conditions $U_6 = U_7$, we obtain from Eqs. 2 and 3 for the reflected shock wave:

$$\delta_4 (P_{73} - 1)(\alpha_4 P_{73} + 1)^{-0.5} = \frac{U_3}{a_3} - a_{53}\, \delta_1 (P_{65} - 1)(\alpha_1 P_{65} + 1)^{-0.5} \qquad (5)$$

and for the reflected wave (from Equations 2 and 4)

$$\delta_4 (P_{73} - 1)(\alpha_4 P_{73} + 1)^{-0.5} = \frac{U_3}{a_3} + a_{53} \frac{1}{\gamma_1 \beta_1} (1 - P_{65}^{\beta_1}) \qquad (6)$$

From the condition $P_6 = P_7$, we obtain

$$P_{73} = P_{65}P_{53} \tag{7}$$

When the reflected diturbances from the contact surface is a Mach wave, that is to say $P_{65} = 1$, we obtain from Eq. (7) that $P_{73} = P_{53}$. In this case from Eqs. (5) and (6) (since $P_2 = P_3$) one obtains

$$\frac{U_3}{a_3} = \delta_4(P_{52} - 1)(\alpha_4 P_{52} + 1)^{-0.5} \tag{8}$$

but from Eq. (1) we may write

$$\frac{U_2}{a_2} = \delta_1(P_{52} - 1)(\alpha_1 P_{52} + 1)^{-0.5} \tag{9}$$

when $U_S = 0$ (U_2 is in the direction opposite to the direction of the shock wave), and, from Eqs. (8), (9) and since $U_2 = U_3$ we obtain:

$$a_{23} = \frac{\delta_4(\alpha_4 P_{52} + 1)^{-0.5}}{\delta_1(\alpha_1 P_{52} + 1)^{-0.5}} = \frac{\gamma_1}{\gamma_4}\left[\frac{1 + \frac{\gamma_1+1}{2\gamma_1}(P_{52} - 1)}{1 + \frac{\gamma_4 + 1}{2\gamma_4}(P_{52} - 1)}\right]^{0.5} \tag{10}$$

Eq. 10 presents the conditions for not producing reflected disturbances from the contact surface. This equation gives the relation between a_{23} and P_{52}.

As P_{52} is a function of P_{41}, Eq. (10) can be used to obtain the relation between a_{23} and P_{41} for "tailored" condition. In the shock tube flow one can derive the following relation:

$$a_{23} = \frac{1}{a_{41}(P_{14}P_{21})^{\beta_4}}\left[\frac{P_{21}(P_{21} + \alpha_1)}{a_1 P_{21} + 1}\right]^{0.5} \tag{11}$$

Since P_{21} is a function of P_{41}, an additional equation is obtained which gives a relation between a_{23} and P_{41}.

Thus Eqs. (10) and (11) define the conditions for no disturbances due to interaction of the reflected shock wave and the contact surface. Equation (11) presents the conditions required in the shock tube in order to obtain the "tailored" value for a_{23}, for a given combination of driver and driven gases at given initial temperatures (the temperature influences the quantity a_{41}). The variation of a_{23} with M_s for air (as the driven gas) and various driver gases is presented in Fig. 3. Thus, at this "tailored" conditions, we obtain between the contact surface and the end of the shock tube a reservoir of high temperature, high pressure air of uniform properties and free of disturbances. By allowing this air to flow through a convergent-divergent nozzle we obtain high Mach number flow in the test section of the shock tunnel. This is done by attaching a nozzle of relatively small throat area (in this case, 4% of the cross section area), at the end of the shock tube. In this case a complete reflection of the incident shock wave still occurs before the shock heated air is expanded through the nozzle.

It should be pointed out that at conditions slightly different from the tailoring conditions, the reflected disturbances from the contact surface are weak and there still exists a reservoir of heated air whose conditions are very nearly uniform. It is pointed out in Ref.[4] that for $5.7 < M_s < 6.3$, the deviation from the tailoring pressure is at most $\pm$ 10%. A theoretical develpment of disturbance strength for the case of deviations from the tailoring conditions may be found in Ref. [5].

2.2. Calculation of the Duration of Flow at Tailored Conditions

The duration of the experiment in the test section of the nozzle is limited by the following factors: The depletion of the reservoir of the hot gas (i.e. the arrival of the contact surface to the entrance of the nozzle), and due to the arrival of the rarefaction wave to the nozzle entrance.

a) Calculation of the Mass Depletion Time

The mass depletion time can be calculated equating the mass flowing out through the nozzle to the mass depletion due to the velocity with which the contact surface is carried towards the nozzle entrance, that is

$$\rho_T A_T U_T = \rho_5 A_5 U_{c.s.} \tag{12}$$

where

$U_{c.s.}$ is the contact surface velocity towards the nozzle.

Since $U_T/a_T = 1$, then

$$\rho_T A_T = \frac{1}{a_T} \rho_5 A_5 U_{c.s.}$$

It follows that:

$$U_{c.s.} = a_T \frac{A_T \rho_T}{A_5 \rho_5} \tag{13}$$

The ratios $\frac{a_T}{a_5}$ and $\frac{\rho_T}{\rho_5}$ can be calculated by assuming that the flow up to the throat is isentropic. Then,

$$U_{c.s.} = a_5 \frac{A_T}{A_5} \left(\frac{1+\gamma}{2}\right)^{-\frac{1+\gamma}{2(\gamma-1)}} \tag{14}$$

For the case in which the air between the contact surface and the end of the shock tube deviates from an ideal gas then the ratio a_5/a_T and

and ρ_5/ρ_T may be obtained from charts for air at thermodynamic equilibrium.

The depletion time, can be now estimated to be,

$$t_{c.s.} = \frac{\ell_{c.s.}}{U_{c.s.}} = \frac{\ell_{c.s.} A_5}{a_5 A_T} \left(\frac{1+\gamma}{2}\right)^{\frac{1+\gamma}{2(\gamma-1)}} \tag{15}$$

where,

$\ell_{c.s.}$ - is the distance of the contact surface from the end of the shock tube and is calculated from the relation

$$\frac{L - \ell_{c.s.}}{U_2} = \frac{L}{U_s} + \frac{\ell_{c.s.}}{U_{s_2}} \tag{16}$$

In this case

$$\ell_{c.s.} = \frac{U_{s_2}}{Us} \frac{U_s - U_{s_2}}{U_{s_2} + U_2} L \tag{17}$$

$$\ell_{c.s.} = \frac{U_{s_2}}{U_s} \frac{U_s - U_2}{U_2 + U_2} \frac{1}{a_5} [(1+\gamma)/2]^{\frac{1+\gamma}{2(\gamma-1)}} \frac{A_5}{A_T} L \tag{18}$$

For specific initial conditions, for which we wish to obtain "tailoring" (i.e. known γ, A_5, a_5, U_2, U_{s_2} and U_s), $t_{c.s.}$ will vary with the ratio A_5/A_T and with L as indicated in Eq. (18). Of course this time is limited by the maximum length of low pressure section which is limited by boundary layer growth.

b) Calculation of the Time for the Arrival of the Rarefaction Wave to the Nozzle.

The rarefaction wave travels with the local speed of sound and its propagation can be calculated by the procedures described in Ref. 1.

2.3. Calculation of Optimum "Tailored"Shock Tube Design

We will define an optimum design for a shock tube that will produce the longest test flow duration in a shock tunnel at "tailored" conditions when the total length of the shock tube is given. This optimum design will exist when the shock tube is so proportioned so that the wave head, the rarefaction wave tail and the contact surface arrive simultaneously at the nozzle entrance position. This condition is presenred in the following relation:

$$\frac{L}{U_s - a_3} = \frac{L'}{a_4} + \frac{L' + L}{\bar{a} + \bar{U}} = L/U_s + B\,\frac{L}{U_{s_2}} + B \times C \times L \qquad (19)$$

time in which the rarefaction wave tail arrives

time in which rarefaction wave head arrives

the time in which the first shock wave arrives at the nozzle

the time in which the reflected shock wave travels the distance between nozzle and the point of encounter with the contact surface

Lost duration due to the depletion of the reservoir

the time in which the contact surface arrives.

where:

$\bar{U}$ - the average velocity at which the reflected rarefaction wave passes through the expansion fan.

$\bar{a}$ - average sonic velocity in the expansion fan

$$B = \frac{U_{s_2}(U_s - U_2)}{U_s(U_{s_2} + U_2)}$$

$$C = \frac{1}{a_5}\frac{A_5}{A_T}\left(\frac{1+\gamma}{2}\right)^{\frac{1+\gamma}{2(\gamma-1)}}$$

Thus, in order to obtain an optimum shock tube we require that the following relation holds for the optimum L,

$$\frac{1}{U_3 - a_3} = B\left[\frac{1}{U_{s_2}} + \frac{1}{a_5}\frac{A_5}{A_T}\left(\frac{1+\gamma}{2}\right)^{\frac{1+\gamma}{2(\gamma-1)}}\right] + \frac{1}{U_s} \tag{20}$$

and in this case the appropriate value of A_5/A_T is:

$$A_5/A_T = a_5\left(\frac{2}{1+\gamma}\right)^{\frac{1+\gamma}{2(\gamma-1)}}\left(\frac{1}{U_{s_2}}\right)\left(\frac{U_s + a_3 - U_3}{U_3 - a_3} \cdot \frac{U_{s_2} + U_2}{U_s - U_2} - 1\right). \tag{21}$$

The additional relation which follows from Eq. (19) is

$$DL' = \left(\frac{B}{U_{s_2}} + BC + \frac{1}{U_s} - \frac{1}{\bar{a} + \bar{U}}\right)L \tag{22}$$

where

$$D = \frac{\bar{a} + \bar{U} + a_4}{(\bar{a} + \bar{U})a_4}$$

Substituting the value of A_5/A_T, obtained from Eq. (21), in Eq. (22) we obtain the relation for optimal lengths of L and L' be,

$$DL' = \left(\frac{1}{U_s - a_3} - \frac{1}{\bar{a} + \bar{U}}\right)L. \tag{23}$$

The application of the present calculation to the shock tube used in this investigation indicates the proper lengths that should be used in order to obtain optimum test flow duration and are shown in Figs. 4 and 5.

2.4. The Additional Reservoir Pressure

In addition to the wave system produced with the bursting of the first diaphragm which was described previously, there is a supplementary shock wave that reaches the region of standing air (region 5) and causes a pressure rise in this region. It should be pointed out that this shock wave appears also when "tailoring" conditions exist. The reason for the appearance of this shock wave was discussed, based on theoretical considerations, in reference (6). This theory will be briefly reviewed herein. In the shock tube driver system presented in Fig. 6 the bursting of the diaphragm due to the high pressure in region 4 will produce an expansion wave which will advance into region 4. This expansion wave causes an unsteady expansion until a new condition (designated as 3u) is attained. This condition will depend on the initial conditions of the driver and driven gases. The equation relating the pressure and velocity in this case will be (relation between the quantities in an expansion wave):

$$\frac{P_{3u}}{P_4} = \left(1 - \frac{\gamma_4 - 1}{2} \frac{U_{34}}{a_4}\right)^{\frac{2\gamma_4}{\gamma_4 - 1}} \tag{24}$$

The expansion of the driver gas through the nozzle at the diaphragm section into region 1 is calculated by the use of the steady flow equations through the nozzle. The relation between the pressure and the velocity is then:

$$\frac{P_{3s}}{P_4} = \left(1 - \frac{\gamma_4 - 1}{2} \left(\frac{U_{35}}{a_4}\right)^2\right)^{\frac{\gamma_4}{\gamma_4 - 1}} \tag{25}$$

where P_{3s} is the condition of the gas following the steady expansion. From Eqs. (24) and (25) we see that if we start from the same initial conditions and attain the same velocity, the resulting pressures P_{3u} and P_{3s} will be different. There

is only one velocity at which these pressures are equal. This velocity can be calculated by equating the pressures in Eqs. (24) and (25).

This condition is called in Ref. (6) the "cross over point". Since this condition does not correspond to the "tailored" condition it is required to introduce an additional unsteady wave which provides the matching boundary conditions in the "tailored" shock tube. This patching process may be accomplished by either a shock wave or a rarefaction wave moving to the right (in the direction of the supersonic nozzle) or to the left respectively.

The conditions which govern the appearance of these waves and their direction depend upon two factors. One condition is the ratio between U_3 or M_s for tailoring and for a cross over point and the second is the area ratio of the nozzle. Reference (6) gives details for various cases. Those of interest for this work are the following: The case where $M_{sT}/M_{sx} < 1$, as is illustrated in the $\ell_{c.s.}U$ diagram of Fig. 7. Presented in this figure are the curves for steady and unsteady expansions. The point A on the unsteady expansion curve corresponds to the velocity and pressure obtained at the tailoring conditions. The corresponding point on the steady expansion line depends on P_4 and on the area ratio of the nozzle. In case where there is no nozzle at the diaphragm section, that is $\delta = 1$, patching is achieved by the expansion wave moving to the left and shock wave moving to the right. This shock wave reaches the resevoir region (region 5) and raises the pressure in this region. This phenomenon is well illustrated in the experimental results obtained in this work. When δ becomes less than 1, the strength of the two waves decreases, and when $\delta = \delta_s$ patched conditions are obtained by only one shock wave which moves to the right. An additional decrease in δ results in two

shock waves, one of which will move to the right and the second to the left. However, the shock wave which moves to the right will become weaker with decreasing δ, while the one which moves to the left with increase in strength. When $\delta = \delta_{ideal}$, patching conditions will be provided by only one shock wave which moves to the left. It is clear that in this case the air behind the reflected shock at the right end of the shock tube will not be disturbed. Additional reduction of δ causes a leftwards moving shock wave and a rightward moving rarefaction wave. This rarefaction wave will reduce the pressure of the air in region 5.

Therefore, it is clear that if we wish to prevent the additional shock wave, we must install an additional nozzle in region 4. A method for the calculation of δ_{ideal} is presented in Reference (6). In the present shock tube using H_2/Air combination and $M_{ST} = 6.0$ the required value for δ is 0.382. This condition was well verified in the experimental program and is discussed in Part III (1).

The installation of a nozzle in region 4 removes the head and the tail of the rarefaction wave which is produced at the bursting of the diaphragm. However, the collision between the first reflected shock wave and the leftward moving patching wave produces a reflected disturbance in the form of a rarefaction wave which moves to the right. The arrival of this rarefaction wave at region 5 will terminate the useful test duration. It is worthwhile to note that the experimental results of this work show that this rarefaction wave arrive at region 5 at about the same time that the first rarefaction wave head would arrive if there were no nozzle. It is important to consider the effect of this additional wave on the shock tube testing. There are cases where it was suggested to incorporate a nozzle at the diaphragm in

order to stop the rarefaction wave (Ref. 7), and therefore eliminate the propagation of this patched wave into region 5. However this additional wave can also be used to increase the pressure in region (5) for certain shock tube geometry (as was done in the present investigation) at a certain loss in test duration.

III. FLOW IN THE HYPERSONIC SHOCK TUNNEL NOZZLE

3.1. Calculation of the Stagnation Conditions (Conditions in Region 5)

From knowledge of M_s and conditions in region 1 of the shock tube it is possible to calculate the conditions behind the reflected shock wave (region 5) which constitute the stagnant air reservoir for the flow in the supersonic nozzle. Agreement between the calculated quantities and the actual values was verified from recordings of the pressure at the end of the shock tube; the experimental results deviate only slightly from those obtained in the theoretical calculations. The thermodynamic properties (assuming equilibrium conditions) were obtained from References 8 and 9. These calculated quantities are correct for the case in which the patching wave is removed by use of a nozzle in region 4 (discussed in Section 2.4). In the case in which the patching wave is not removed, it was found experimentally that the final pressure region 5 was larger by factor of 1.6 than that in a system in which the patching wave is removed. It should be remembered that this pressure rise results from two waves, the patching wave which passes through region 5 and the reflection of this wave from end of the shock tube. If we assume that all of the rise in pressure results from one wave only then for this pressure rise the corresponding rise in the total enthalpy and in the

stagnation temperature is only 10%. Therefore, an average value for the total enthalpy may be taken in the reservoir with or without patching wave with reasonable accuracy. Of course the pressure and the density will be different in the two cases. Table 1 presents typical shock tube conditions for the operation of the tailored shock tunnel. At these conditions there exists (Fig. 8, which was taken from Reference (10))only one significant reaction in the air, i.e. the dissociation of the oxygen molecules into atoms.

The steady flow in the supersonic nozzle (after the flow starting process) can be assumed to be isentropic, while the flow may be either in thermodynamic equilibrium or fronzen conditions.

A computer chart for the calculation of the equilibrium flow knowing the reservoir conditions is presented in Fig. 9. Results for isentropic thermodynamic equilibrium flow in hypersonic nozzle are presented in Ref. 11.

TABLE I

M_s	P mm Hg	T_1 °K	Bhu/lb	T_{oK}	Z	γ	μ $\frac{kg\ sec}{m^2}$	P_{ata}		ρ $\frac{Kg\ Sec^2}{m^4}$	
6	35	300	2100	3500	1.03	1.21	8.4×10^{-6}	14.8 without patching wave	23.5 with patching wave	0.15 without patching wave	0.22 with patching wave

3.2. The Starting Process in the Shock Tunnel Nozzle

Prior to the start of the experiment a cellophane diaphragm is inserted between the shock tube and the hypersonic nozzle. The air pressure in the nozzle is lower than that in the shock tube. It is clear that if the initial pressure in the nozzle will be higher than the static pressure of the steady hypersonic flow then the proper flow in the nozzle cannot be established (Ref. 15).

The flow immediately after bursting of the diaphragm is similar to the flow immediately after bursting of the diaphragm in the shock tube. Here also, due to the pressure difference across diaphragm, a shock wave is produced which travels to the right (in the direction of the dump tank) and a rarefaction wave which moves to the left (in the direction of the shock tube). This wave structure associated with the flow starting phenomena in the hypersonic nozzle is very complicated due to the variation in the cross-sectional area of the nozzle and due to the secondary disturbances produced following interaction between the shock wave and the rarefaction wave. Fortunately, quantitative evaluation is not of interest since the main requirement is that these disturbances will be swept downstream as quickly as possible. Experimental results in Refs. 15 and 16 show that the greater the initial pressure ratio between the shock tube and the hypersonic nozzle the shorter is the time during which these disturbances are swept away.

Flow starting disturbances which occur in the shock tube may be qualitatively explained with the aid of a p - U diagram similar to that used for the explanation of the patching wave disturbances in the shock tube (Section 2.4). It is not possible to connect the initial pressure in the nozzle and the static pressure of

the steady flow by a rightward moving shock wave and a leftward moving rarefaction wave only. An additional unsteady phenomenon is required, a rarefaction wave or shock wave. When the initial pressure in the shock tunnel nozzle is low, patching between the steady and the unsteady flows is accommplished by a leftward moving rarefaction wave and a rightward moving shock wave. As the initial pressure in the nozzle is increased the leftward moving disturbance is transformed from the rarefaction wave to a shock wave. It should be noted that while these disturbances move with respect to each other, they are all swept rightwards by the air flowing in this direction at hypersonic speed. The weaker these disturbances are and the higher the flow velocity is, these disturbances are then swept faster passed the test section. The duration of the passage of these disturbances of the nozzle beyond test section is actually the lost test time due to the starting process.

In the case of frozen flow, calculations for the flow parameters at various reservoir conditions and various Mach numbers for which the flow freezes are presented in Ref. 12.

3.3. The Calculation of the Stagnation Point Heat Transfer in the Hypersonic Shock Tunnel Flow.

The stagnation point heat transfer in hypersonic flow has been calculated in References 13 and 14, and can be presented in the following equation:

$$\dot{q}_w = 0.763\ Pr^{-0.6}(\rho_s\mu_s)^{0.5}\left(\frac{\rho_w\mu_w}{\rho_s\mu_s}\right)^{0.1}\left[\left(\frac{dU}{ds}\right)_s\right]^{0.5}(h_s - h_w)\left[1 + (L^c - 1)\frac{h_c}{h_s}\right] \tag{26}$$

where:

For frozen flow - $c = 0.63$.

For equilibrium flow - $c = 0.52$.

and $h_c = h_A^o \alpha_s$

Since L is close to 1, the terms h_c/h_s is less than one and α_s is small due to the relatively high pressure at the stagnation point, the equation may be written in the form:

$$\dot{q}_w = 0.765\ Pr^{-0.6} (\rho_s \mu_s)^{0.5} \left(\frac{\rho_w \mu_w}{\rho_s \mu_s}\right)^{0.1} \left(\frac{dU}{ds}\right)_s (h_s - h_w) \qquad (27)$$

The velocity gradient at the stagnation point of a sphere will be:

$$\left(\frac{dU}{ds}\right)_s = \frac{A}{r_o} \left(\frac{p_s - p}{\rho_s}\right)^{0.5} \qquad (28)$$

The value of A is 1.41 for Newtonian pressure distribution on the sphere and p is then the static pressure of the undisturbed flow. If the flow about the sphere is assumed to be like the incompressible potential solution then $A = 2.12$ and p is the static pressure behind the detached shock wave. The evaluation of these values is presented in Appendix A.

For small values of h_w/h_s, which is the situation in shock tunnel (since the model is at room temperature) then

$\left(\frac{\rho_w \mu_w}{\rho_s \mu_s}\right)^{0.5} \simeq 1$ and ,

$$\dot{q}_w = 0.763\ (Pr^{-0.6}) r_o^{-0.5} A^{0.5} \mu_s^{0.5} (\rho_s (p_s - p))^{0.25} (h_s - h_w) \qquad (29)$$

Let $K = 0.763\ Pr^{-0.6}\ A^{0.5}$, and since $(\frac{\rho_s}{\rho_5})^{0.25} \simeq (\frac{p_s}{p_5})^{0.25}$, then

$$\dot{q}_w = K r_o^{-0.5} \mu_s^{0.5} (\rho_5 p_5)^{0.25} (\frac{p_s}{p_5} \cdot \frac{(p_s - p)}{p_5})^{0.25} (h_s - h_w) \qquad (30)$$

Using the relation

$$(\rho_1 p_1)^{0.25} = (\frac{p_1^2}{gRT_1})^{0.25}$$

the following equation is obtained (based on the known conditions in the shock tunnel),

$$\dot{q}_w = K r_o^{-0.5}\ \mu_s^{0.5} (\frac{\rho_5 p_5}{\rho_1 p_1})^{0.25} p_1^{0.5} (\frac{1}{gRT_1})^{0.25} [(\frac{p_s}{p_5})(\frac{p_s}{p_5} - \frac{p}{p_5})]^{0.25} (h_s - h_w) \qquad (31)$$

The quantity $\dot{q}_w \frac{r_o^{0.5}}{p_1^{0.5}}$ which is calculated from Eq. (31) for air in thermodynamic equilibrium as a function of the flow Mach number in the shock tunnel at various stagnation enthalpy levels is shown in Fig. 10.

IV. THE EXPERIMENTAL SYSTEM

4.1. The Shock Tunnel

The main part of the shock tunnel and its overall dimensions are shown in Fig. 11. The shock tunnel consists of two main parts: the shock tube and the hypersonic nozzle. Photographs of the shock tunnel are presented in Fig. 12. The high pressure section of the shock tube consists of a circular cross-section with an internal diameter of 80mm. and an external diameter of 115 mm. and is designed for operation to internal pressures of 200 atm. This tube is made of steel and is 2 meters long. One end of the tube is closed by a flange to which the driver gas feed system is connected. The other end is connected to the low pressure channel and at this end the diaphragm is also located. The low pressure channel is 7 meters long with a square 75 x 75 mm. cross-section. Although this low pressure section is limited in the pressure range of its operation, the two dimensional flow present in the square cross-section is preferred for aerodynamic studies when it is used as a shock tube. A test section is located near the end of this tube with windows through which it is possible to install models for research in the shock tube flow. Various measurements can be made with transducers installed through several ports which are placed along the last three meters of the shock tube. A convergent divergent hypersonic nozzle is installed at the end of the shock tube. The convergent section reduces the cross-section area from the 75 x 75mm. channel to a throat of 15 x 15 mm. Downstream of the throat provisions are made for holding the cellophane diaphragms which separate the shock tube initial pressure from that of the hypersonic nozzle. The divergent section is composed of two sections.

In the first section, the nozzle diverges to the area ratio, $A/A^* = 78$. This section starts in a horizontal position and ends with a deflection of 10 degrees through a deflection plate. This deflector plate is introduced in order to centifuge out the cellophane particles which are carried with the flow and thereby reduce the damage to models in the test section. It is worth noting that this arrangement was found to be efficient since heat transfer gauges, which are very sensitive to particle damage, were almost undamaged during the progress of these experiments. The second section of the nozzle, which protrudes slightly into the first section, starts with a cross-sectional area smaller than that at the end of the first section; this permits the removal of the boundary layer of the first section and makes it possible to obtain an area ratio, A/A^* larger than would be possible in a one stage nozzle . The width of this second section is constant at 200 mm. while the height is varied by a wedge type nozzle. The wedge angle can be varied, so that it is possible to vary the entrance area to the test section and therefore the flow properties in this section. Fig. 13 shows the second section of the nozzle (with the first section removed) and the associated equipment including the 0.25 m^3 dump tank which is connected to the end of the hypersonic nozzle, the boundary layer removal system, the diffusion pump etc. The test section is incorporated into the second section of the nozzle, and a model support strut is installed behind the test section.

The Low Pressure System includes a Edwards-Kinney vacuum pump, KD 110, which is connected to the low pressure channel of the shock tube. This tube can be evaluated to less than 1 mm. Hg abs. The low pressure system for the hypersonic nozzle is composed of three vacuum pumps connected in series. These include a

rotary vacuum pump, Leybold S-60, a Leybold Ruvac 25, of the Roots-Blower type and an oil diffusion pump, Edward-Speedviac F-603. With this system the pressure of the nozzle section would be held at approximately 20 μ Hg. abs. The time required to reach the desired low pressure in the low pressure channel was several minutes and in the hypersonic nozzle, approximately 15 minutes.

The High Pressure Gas Supply System uses commercial bottled high pressure hydrogen or the laboratory high pressure air supply for air driven operation. Gas flow to the shock tube is regulated by a valve located on the control panel, where the compression chamber pressure is indicated on a pressure gage. This valve is hand operated and is closed manually after bursting of the diaphragm.

4.2. The Instrumentation System

The block diagram of the instrumentation system is presented in Fig. 14. The gauges which record the measured pressures prior to the experiment are mounted on the control panel. These measuring instruments are: 1. The pressure in the high pressure-tube-measured by a pressure gauge. 2. The low pressure in the low pressure channel. 3. The low pressure in the supersonic nozzle. 4. Room Temperature. The output of the model instrumemtation is recorded on Tetronix oscilloscopes models 535, 555 and 565 which were operated in a single sweep mode. The data was photographed by Polaroid cameras.

Pressure Measurements

Pressures were measured by piezoelectric transducers manufactured by the Kistler Company. Performance details of the transducers are given in the following Table:

Location & Type of Measure-ment	Model No.	Typical Pressure Measured psi	Range of tranducers psi	Elec. Output pcb/psi	Response Time μ sec	Natural Frequency cps	External dimensions (length x diameter) inches
Static pressure at the end of the shock tube	601	300	10-3000	1.2	3	130,000	0.25 x 0.6
Total pressure behind the shock wave in the test section	603	5	0-3000	0.37	1	400,000	0.25 x 0.45
Static pressure in the test section	606	0.05	0-30	4.4	3	130,000	0.5 x 1.25

It is immediately obvious from the table that except for the transducers at the end of the shock tube, the others operated in the lower portion of their measurement range, this results in a relatively low signal-to-noise ratio. In order to improve the signal-to-noise ratio passive electrical filters were installed. These filters had two filter-

ing levels, one removes noise above a frequency of 1000 Hz and the second removes noise above 3000 Hz. The lag time in the pressure measurements due to these filters is approximately 100 μsec. which is tolerable in the shock tunnel measurements. The pressure transducers were connected through the charge amplifiers (Kistler Model 504 amplifiers) to the oscilloscope. The total pressure gages were mounted in a rake which is shown in Fig. 15. The rake mounting arrangement allows rotation and movement of the rake in the direction of the longitudinal tunnel axis. This arrangement enables the mapping of the total pressures at various angular positions and at various axial positions of the test section.

The static pressure was measured on the test section side wall through specially made measuring ports in a window. The pressure transducer is installed in a plug which is mounted on O-rings, an arrangements which also provided vibration isolation of the pressure gages from the tunnel. Since all of the plugs were interchangeable, it was possible to measure the static pressure at various positions along the axis of the test section and at various heights in the test section.

It was found necessary to protect the surfaces of the piezoelectric pressure transducers by covering the face of each gauge with a thin layer of thermal insulation material, such as vacuum grease, so that the gauge is not exposed directly to the hot ionized air. This protective coating eliminated stray output and resulted in signals sensitive to the pressure variations only. This phenomena is mentioned also in Reference 17.

Heat Transfer Measurements

Heat transfer measurements were made with the thin platinum film resistance gauges. These gauges are made by sputtering a thin layer of platinum on pyrex glass. The output voltage variations as a function of temperature change is given by the relation $\Delta V = I_o(R - R_o) = I_o R_o \alpha \Delta T$. Response time of these gauges is smaller than a microsecond. The gauges, their preparation and calibration is described in Reference 18. These gauges were used in this work for the following measurements: (1) measurements of the stagnation point heat transfer rates in the hypersonic flow in the shock tunnel test section and (2) detectors of the incident shock wave for the shock velocity measurements in the shock tube.

The gauges that were used to measure heat transfer rates were sputtered on pyrex glass segments that were cut from the hemispherical head of a 15 mm. diameter hemispherical capped test tubes. The gauges were then inserted into steel 15mm diameter hemispherical recepticles so that smooth hemisphere nosed probes were obtained. The sensitive film on the gauge was such that the stagnation point heat transfer rate variation of the portion of the half sphere which it covered was negligible, since the heat transfer rate near the stagnation points falls of rather slowly (Ref. 19). The dimensions of the platinum film on these gauges is about 5 mm. long and 1 mm wide. A description of the gauge calibration and of the calibration system used in this work may be found in Ref. (20). The hemispheres are mounted on a rake which is similar to the one used for the total pressure measurements, except for the instrumented probe section of course. This rake is shown in Fig. 16.

The data reduction follows the procedures developed in this laboratory, and others (References 19 and 20) to determine the heat transfer rates from the thin film gauges output. The electronic equipment used in this work (Oscilloscopes, counters, charge amplifiers, pulse amplifiers and electric current supplies) are shown in Fig. 17.

V. EXPERIMENTAL RESULTS

5.1. Experimental Results in the Shock Tube

The measurements in the shock tube are compared with the theoretical calculations of the flow in the shock tube with reasonably good agreement. The incident shock wave attenuation is measured using four thin film gauges positioned in the shock tube low pressure channel as follows: two of the gauges were located permanently at stations 1 and 2 of the shock tube (see Fig. 18) and the other two were moved to the various other measuring stations. It can be seen in Fig. 18 that the Mach number of the shock wave is attenuated by 1.5% to 2% in the 2 meters of the instrumented section, therefore, for the 7 meter shock tube length the attenuation will be no greater than 5% to 7%. This shows that there is only a slight influence of the boundary layer growth on the shock wave velocity in the present shock tube. Data scatter in this graph may be attributed to the fact that of the two counters that were used the Beckman 7360 had an accuracy of one μsec and the Beckman 6146 had an accuracy of 0.1 μsec. Since a typical reading of the counters was approximately 150 μsec. then the error caused by the 6146 counter was negligible and that caused by the 7360 counter was about 0.3%.

Fig. 19 includes the compilation of results for the relation between the pressure ratio across the diaphragm, p_4/p_1, and incident shock wave Mach number, M_s, as measured between stations 1 and 2 (see Fig. 18). As seen in this figure, the experimental data scatter is large. It is possible to relate the scatter to the non-uniformity of the diaphragm material and the non-uniformity of the diaphragm scribbing process and as a result of this the non uniformity in the diaphragm opening and bursting process. In spite of the wide scatter it is possible

to see that the pressure ratio required in order to obtain a given M_s is considerably larger than that predicted by the ideal gas theory. The pressure measurements at the end of the shock tube are presented in Figs. 20 and 21, and a typical pressure gauge output obtained on the oscilloscope camera is shown in Fig. 22. It can be seen that at increasing shock Mach numbers the pressure in region 2, p_2/p_1 increases above that predicted by the ideal gas theory (Fig. 20). At tailoring conditions, for hydrogen driver gas, (i.e. at $M_s = 6.0$) this deviation is still very small (less than 10%). The measurements of p_5/p_1 as a function of M_s are presented in Fig. 21. It is seen that the experimentally obtained values are in good agreement (at least up to the tailoring conditions) with the theoretical results for $\gamma = 1.4$, and somewhat lower than those predicted for a real gas. Since the measured p_2/p_1 values were higher than the theoretical values, then the reflected shock wave must be weaker than that predicted by the theory.

Fig.23 shows the pressure of the air at reservoir conditions as measured by the pressure gauge at the end of the shock tube. The lower trace corresponds to a measurement without a nozzle in the high pressure region and the upper one with a nozzle there. From these figures it is seen that insertion of the nozzle in the high pressure region results in a lower pressure by preventing production of the additional shock wave which raises the pressure. It is seen that p_2 and p_5 are equal in both cases; the final pressure, p_e, of the stagnant air without a nozzle in the high pressure region, is approximately 1.6 times that which is obtained with a nozzle. It should be noted that the available duration for testing (the time during which constant pressure exists) is several hundred micro-

seconds longer for runs with the nozzle compared to those without the nozzle. As the pressure gauges that were located in the supersonic nozzle were operating at the lowest limit of their range causing a very low signal-to-noise ratio and since pressure in the supersonic nozzle is a direct function of p_e, it was preferable in most of the present experiments to operate without this nozzle in the high pressure region in spite of the fact that by operating in this manner the useful test duration was reduced somewhat.

A phenomenon which was not predicted by the theory and which was present in all the experiments is seen well in Fig. 23. This is the momentary pressure drop immediately following the reflected shock wave. This drop lasts about 500 μsec and afterwards the pressure returns to its previous value. In an experiment in which the end of the shock tube was completely blocked the same phenomenon was obtained. Therefore, the phenomenon cannot be related to the rarefaction waves produced with bursting of the diaphragm at the entrance to the hypersonic nozzle and to the air flow into the hypersonic nozzle. An explanation for this phenomenon, which is also mentioned in Ref. (4), has not been found.

The pressure measurements enable as well the evaluation of the lengths of time of the various processes in the shock tube which can be compared with the theoretically calculated processes as shown in Fig. 4. The duration of flow in region 2 was measured at the condition of Fig. 22 to be 43 μsec, which is in good agreement with the calculated value. The time of arrival of the rarefaction wave for the conditions of Fig.23 is 2680 μsec after the arrival of the incident shock wave. This value is larger than the calculated value of 2050 μsec. However, it should be mentioned that the calculation of the arrival time of the head

rarefaction wave at the right end of the shock tube is very inaccurate since the calculation neglects changes in thermodynamic properties, and therefore, in the sonic velocity in the gas following interaction between the shock and rarefaction waves travelling in the tube.

5.2. Experimental Results in the Shock Tunnel

Calibration of the supersonic nozzle is made at two nozzle positions: position A (area ratio $A/A^* = 225$) and position B (area ratio $A/A^* = 500$) (see Fig. 25). At each nozzle setting the total pressures in the test section is measured with the pressure rake and the stagnation point heat transfer rate with the thin film resistance gages rake. The measurements are done at two stations on the nozzle longitudinal axis, stations 1 and 2, as shown in Fig. 25. At each of these stations horizontal and vertical distributions are measured. Static pressure gauges are positioned at various points on the sidewall window of the test section, and both axial and vertical static pressure distributions in the test section were measured.

The pressure gauge output is determined directly from the photographs of the pressure traces by measurement of the difference between the pressure during the experiment and the initial pressure. From knowledge of the nozzle initial pressure it is possible to determine the value of the absolute pressure during the experiment.

The heat transfer rate is determined using the following relation:

$$\dot{q} = [\pi(\rho C_p k)_b]^{0.5} \frac{\Delta T}{\sqrt{t}} = \frac{\pi}{2} \frac{(\rho C_p k)^{0.5}}{\alpha} \left(\frac{1}{R_o I_o}\right) \frac{\Delta V}{\sqrt{t}}$$

The parameter $\frac{\alpha}{(\rho C_p k)_b^{0.5}}$ is the calibration coefficient of the gauge which is obtained during its calibration, I_o and R_o are measured, and then $\dot{q}$ is determined. In this work a computer program was used to find the best fit parabola for the measured values of ΔV vs. t, thus determining $\frac{\Delta V}{t}$

Fig. 26a shows the trace of the total pressure behind the shock wave for a pressure ratio $p_1/p_i = 610$. This pressure ratio gives an indication of the low pressure in the tunnel prior to the experiment since the pressure p_1 was approximately 35 mm Hg for all of the experiments. The expansion fan produced after bursting of the cellophane diaphragm is seen in this figure. Fig. 26b also shows the trace of the total pressure behind the shock wave, however, in this case the pressure ratio was $p_1/p_i = 185$. In this case it is seen that the expansion fan at the beginning of the flow passes through a shock wave which cause a momentary pressure rise. Fig. 26c shows the static pressure trace. Typical output of the stagnation point heat transfer rate are shown in Fig. 27. The influence of the starting phenomenon on the test duration is demonstrated in Fig. 28. Since the static pressure for the nozzle in position B is considerably lower than that of position A the duration of the starting process in this nozzle at position A is much shorter and steady conditions are obtained from t = 1.8 to 2.9 msec, while with the nozzle at position B the steady conditions are obtained only after 2.4msec to 3.0msec. These traces are typical of all the experiments that were performed in the hypersonic nozzle.

Figs. 29 to 32 summarize the total pressure distribution measured in the test section. It is seen that in both nozzle positions the horizontal pressure

distribution is uniform and the boundary layer is relatively thin (Figs. 29 and 31). When the nozzle is in position A, two pressure levels appear in the vertical distribution (Fig. 30), in the lower half of the cross-section the total pressure behind the shock wave is higher than that in the upper half. The boundary layer in this case is also relatively thin. The vertical mapping with the nozzle in position B(Fig. 32) shows a uniform pressure distribution in the center of the cross-section, however, the pressure drop away from the center core indicates a relatively thick boundary layer.

Vertical mappings of the static pressure in the test section (Figs. 33 and 34) verify the phenomenon observed with the total pressure gauges. The static pressure mapping of position A, Fig. 33, also shows two pressure levels, the higher level being located in the lower half of the section. Fig. 34 shows a uniform vertical static pressure distribution when the nozzle is in position B. The stagnation point heat transfer distribution in the test section, shown in Figures 35 to 38, is very similar to the pressure distributions. The horizontal heat transfer distributions are uniform for both nozzle position, as seen in Figs. 35 and 37. In both of these nozzle positions there is an indication of a thin boundary layer. In the vertical heat transfer rate distributions for the nozzle position A, two heat transfer rate levels are found where the higher level is found in the lower part of the section (although the phenomenon is smaller than in the pressure distribution case). The uniform core at the center of the test section is narrower in the heat transfer measurements than that obtained from the total pressure measurements.

The static and total pressure measurements enable the determination of the test section Mach number distribution. In this case an equilibrium expansion in the nozzle was assumed for the Mach number evaluation.

For nozzle position B there is very good agreement between the Mach number that was obtained from the total pressure measurements behind the shock wave and that obtained from the static pressure measurements, (M = 6.9 to 7.0 was obtained).

The nozzle at position A has a somewhat non uniform flow due probably to various disturbances which are due to the asymetric wedge type nozzle shape. Therefore for the nozzle in position A the Mach numbers obtained from the total pressure measurements are different from those obtained from the static pressure measurements. These differences indicate a Mach number of about 5.1 in the lower part of the nozzle and 5.7 in the upper part.

Good agreement is obtained when the heat transfer rates that were obtained in the experiments (Figs. 35 to 38) are compared, with the theoretical results (Figs. 10 and 10A) when the flow Mach number is the one that is determined from the pressure measurements and the velocity gradient at the stagnation point $(\frac{dU}{ds})_s$ is calculated using the potential flow distribution around a sphere (see Appendix A). When this velocity gradient term is calculated according to the Newtonian approximation (also found in Appendix A), the experimental results are 40% lower than the theoretical results at the assumed flow Mach number.

VI. SUMMARY AND CONCLUSIONS

The present shock tunnel was added to an existing shock tube in which the ratio between the lengths of the driver gas section and the driven gas section is suitable for work in the shock tube itself since the driven gas section is long and gives a relatively long time between the incident shock wave and the contact surface (Region 2). However, this length ratio is not the optimal ratio for maximum flow duration in the hypersonic nozzle for the hydrogen/air tailoring conditions. It is shown that by changing this length ratio it will be possible to increase the flow duration in the hypersonic nozzle by a factor of two. It is also shown that high initial pressures are very advantageous since they enable reasonable pressures in the hypersonic nozzle test section. The extremely simple nozzle design used in the present shock tunnel enabled easy regulation of the flow Mach number in the test section and surprisingly good flow properties.

This work indicates that it is possible to use the present shock tunnel for aerodynamic measurements at reasonably high stagnation enthalpies (2000 Btu/lb. for hydrogen/air at tailoring conditions) and high Mach numbers. Test time of steady flow duration in the hypersonic nozzle is at least 500μsec. for the Mach 7 nozzle and about 1μsec. for the Mach 5.5 nozzle. A more optimal design will result in about 2 msec. of steady flow in the hypersonic nozzle. The uniform flow core in the nozzle is about 8 cm high and about 16 cm wide, so that relatively large models can be used in this test section for hypersonic testing.

The average properties in the test section for the two nozzle positions determined in the present investigation are:

Nozzle Position	Nominal Mach Number	P ata (mm Hg)	P_{o2} ata	T ^{o}K	U m/sec	Re/m 1/m
A	5.5	6.8×10^{-3} (5)	0.33	550	2850	3.6×10^{5}
B	7	2.5×10^{-3} (2)	0.16	420	2900	2.1×10^{5}

APPENDIX A

CALCULATION OF THE VELOCITY GRADIENT AT THE STAGNATION POINT OF A SPHERE IN HYPERSONIC FLOW

Since the flow behind the strong detached shock wave is low subsonic flow, it is possible to assume that the density at the stagnation region is constant and equal the density at the stagnation point. In this case the velocity distribution in the stagnation region can be calculated from the subsonic incompressible potential solution of the flow over a sphere.

The potential equation is then

$$\phi = -\frac{U}{2} r^2 \sin^2\theta + \frac{U r_o^3}{2r} \sin^2\theta$$

where: U - freestream flow velocity in this case the velocity (behind the shock wave)

r_o - sphere radius

Then:

$$U_r = \frac{1}{r^2 \sin\theta} \frac{\partial\phi}{\partial\theta}$$

$$U_\theta = \frac{1}{r \sin\theta} \frac{\partial\phi}{\partial r}$$

where:

U_r = radial velocity

U_θ = velocity in direction θ

On the sphere surface, $r = r_o$, $U_r = 0$ and $U_\theta = 3/2\ U \sin\theta$

Since

$$d_s = r_o d\theta$$

and :

$$\frac{dU_o}{ds} = \frac{dU_o}{d\theta}\ \frac{d\theta}{ds}\ \frac{3}{2r_o} U \cos\theta$$

at the stagnation point

$$\left(\frac{dU}{ds}\right)_s = \frac{3}{2r_o} U$$

From this relation:

$$U = \left[\frac{2(p_s - p)}{\rho_s}\right]^{0.5}$$

where:

p - static pressure behind a shock wave

p_s - stagnation pressure behind a shock wave.

So that:

$$\left(\frac{dU}{ds}\right)_s = \frac{3}{2r_o}\left[2\ \frac{p_s - p}{\rho_s}\right]^{0.5} = \frac{3}{2r_o}\left[\frac{p_s - p}{\rho_s}\right]^{0.5}$$

The velocity gradient can be also estimated assuming the Newtonian pressure distribution as follows:

$$C_{ps} = \frac{p - p_\infty}{1/2\ \rho_\infty U_\infty^2} = C_{p_{max}} (1 - \sin^2\theta)$$

$$C_{p_{max}} = \frac{p_s - p_\infty}{1/2\ \rho_\infty U_\infty^2}$$

where:

p - static pressure on the sphere surface, static pressure behind a shock wave.

p_s - stagnation pressure behind a shock wave

p_∞ - freestream pressure in front of a shock wave

U_∞ - freestream velocity in front of a shock wave

and the velocity gradient at the stagnation point is in this case:

$$\left(\frac{dU}{ds}\right)_s = 1/r_o \left[\frac{2(p_s - p)}{\rho_s}\right]^{0.5}$$

REFERENCES

1. Glass,I.I. and Hall, J. - Handbook of supersonic aerodynamics, section 18 - shock tubes, - NAVROD Rep. 1488.
2. Rabinowicz, J. - Aerodynamic studies in the shock tube, GALCIT Hypersonic Research Project Memoramdun No.38, June 10, 1957.
3. Wittliff, C.E., Wilson, M.R., and Hertzberg, A. - The tailored interface hypersonic shock tunnel, Journal of Aeronautical Science, Vol. 26, pp.219, 1959.
4. Holder, D.W., and Schulz, D.L. - On the flow in a reflected shock tunnel, R & M Report No. 3265, August 1960.
5. Flagg, R.F. - Detail analysis of shock tube tailored conditions, AVCO Technical Memorandum, RAD-TM-63-64, September 1963,
6. Flagg, R.F., - A theoretical analysis of the driver reservoir method of driving hypersonic shock tunnels, UTIAS Technical Note No. 98, April 1965.
7. Schultz, D.L. - A note on the use of steady expansions in shock tubes and shock tunnels, Aero Research Council Report c.p. 558, January 1961.
8. Lewis, C.H., and Burgess, E.G. - Charts of normal shock wave properties in imperfect air, AEDC Technical Documentory Report AEDC-TDR-64-43,March,1964.
9. Hansen, C.F. - Approximation for the thermodynamic and transport properties of high temperature air, NASA TR R-50, 1959.
10. Hansen, C.F. - Approximations for the thermodynamic and transport properties of high air, NACA TN 4150, March 1958.
11. Jorgensen, L.H. and Baum, G.M. - Charts for equilibrium flow properties of air in hypervelocity nozzles, NASA TN D-1333, September 1962.

REFERENCES (CONTD')

12. Yoshikawa, K.K. and Katzen, E.D. - Charts for air flow properties in equilibrium and frozen flows in hypervelocity nozzles, NASA TN D-693, April 1961.

13. Dorrance W.H. - Viscous hypersonic flow, McGraw-Hill.

14. Fay J.A., and Riddell, F.R. - Theory of stagnation point heat transfer in dissociated air, Journal of the Aeronautical Sciences Volume 25 No. 2, pp.73-85, February 1969.

15. Henshall, B.D. - Experimental results from the NPL hypersonic shock tunnel, "Hypersonic Flow" Proceedings of the 11th Symposium of the Colston Research Society, pp.1-44, April 1959.

16. Smith, C.E., - The Starting process in a hypersonic nozzle, University of Oxford Report No. 1000, July 1965.

17. Chan, Y.Y., Mason R.P. and Reddy, N.M. - Instrumentation and calibration of UTIS 11in x 15in hypersonic shock tunnels, UTIS TN 91, June 1965.

18. Rabinowicz, J., Jessey, M.E., Barch, C.A. - Resistance thermometer for heat transfer measurement in shock tube, GALCIT Hypersonic Research Project Memorandum No. 33, July 1956.

19. Lees, L. - Laminar heat transfer over blunt nosed bodies at hypersonic flight speed. The Jet Propulsion Journal Vol. 26, No.4, pp.259-269, August, 1956.

20. Seginer, A., Cohen, A. and Rom, J. - Calibration of thin film resistance thermometer for heat flux measurements in the shock tube. Israel Journal of Technology, Vol. 3. No. 1, pp. 25-30, 1965.

21. Skinner, G.T. - Analog network to convert surface temperature to heat flux. A.R.S. Journal Vol. No. 30, pp.569-570, June 1960.

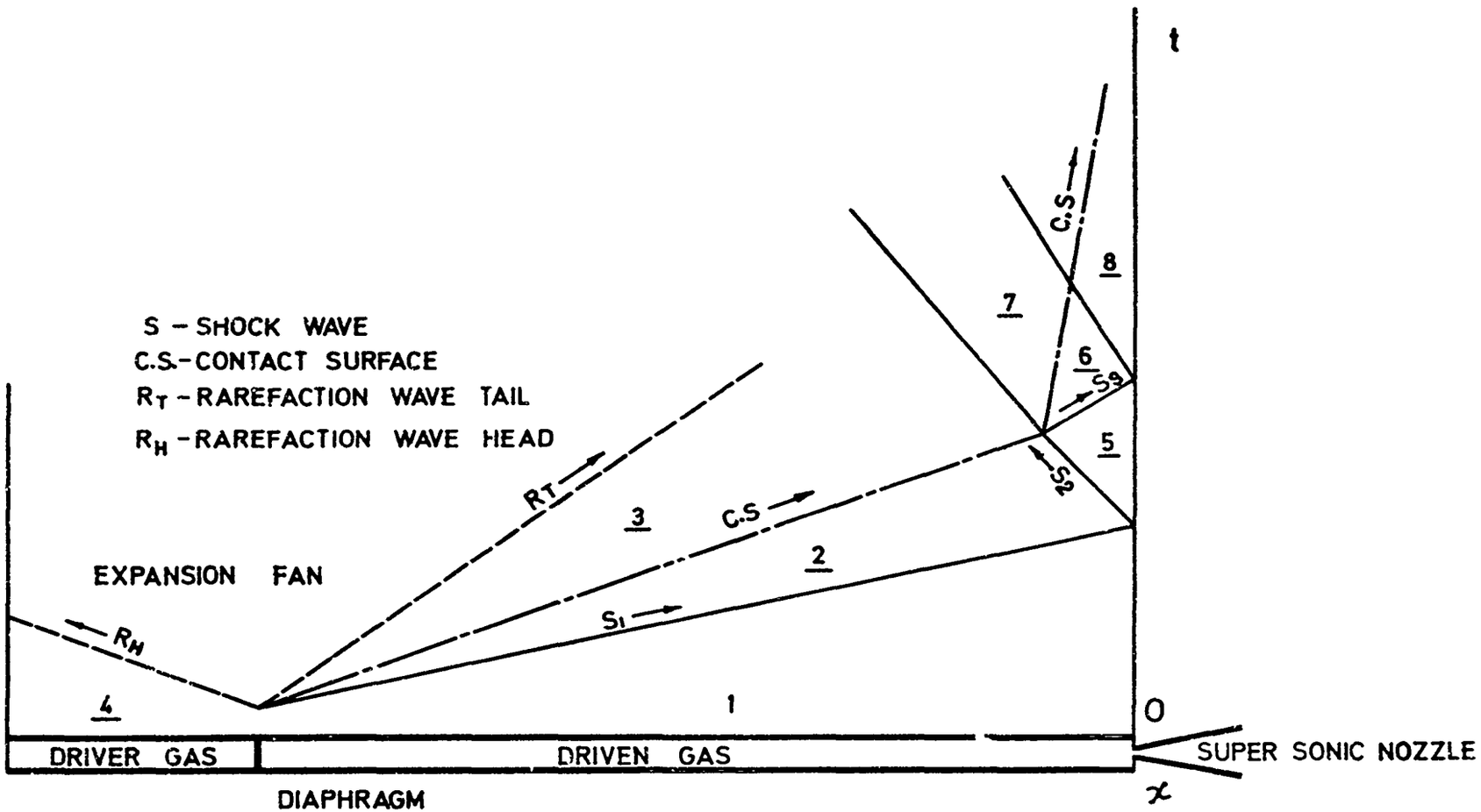

FIG. NO. 1: FLOW REGIONS IN A SHOCK TUBE.

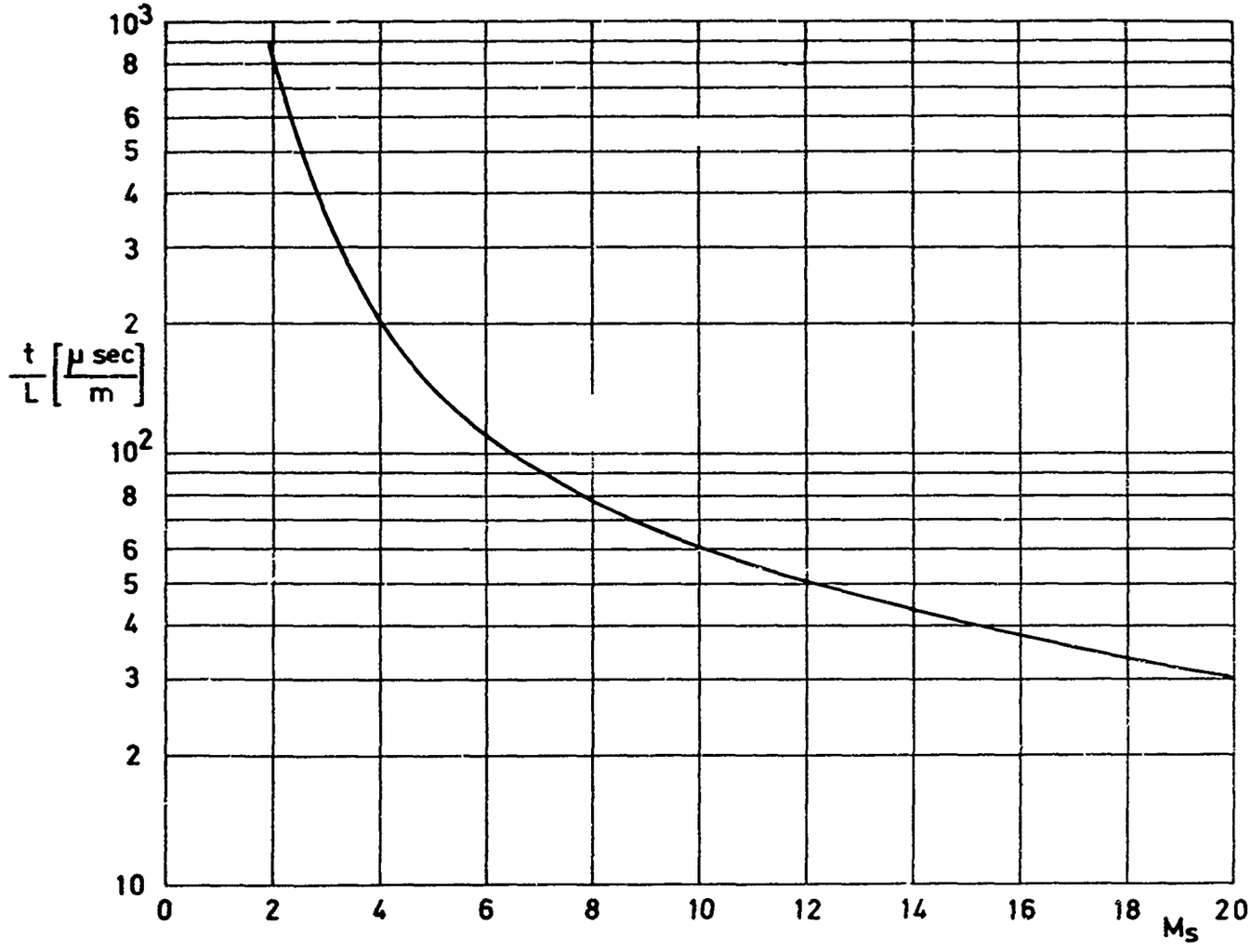

FIG. NO. 2: HOT FLOW DURATION, FOR UNIT LENGTH, IN SHOCK TUBE.

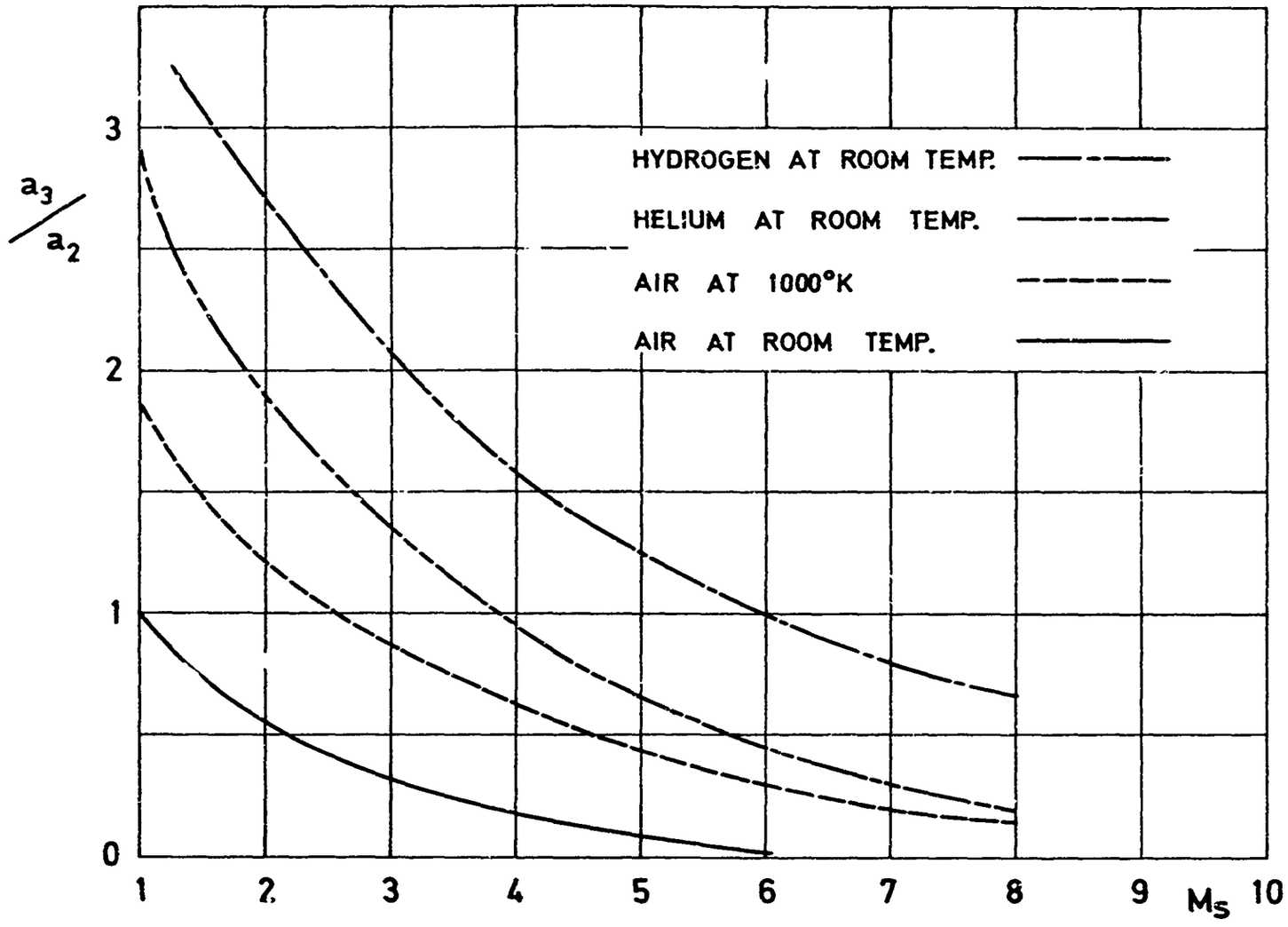

FIG. NO. 3: a_3/a_2 VS M_S FOR AIR AS A DRIVEN GAS AND DIFFERANT DRIVER GASES.

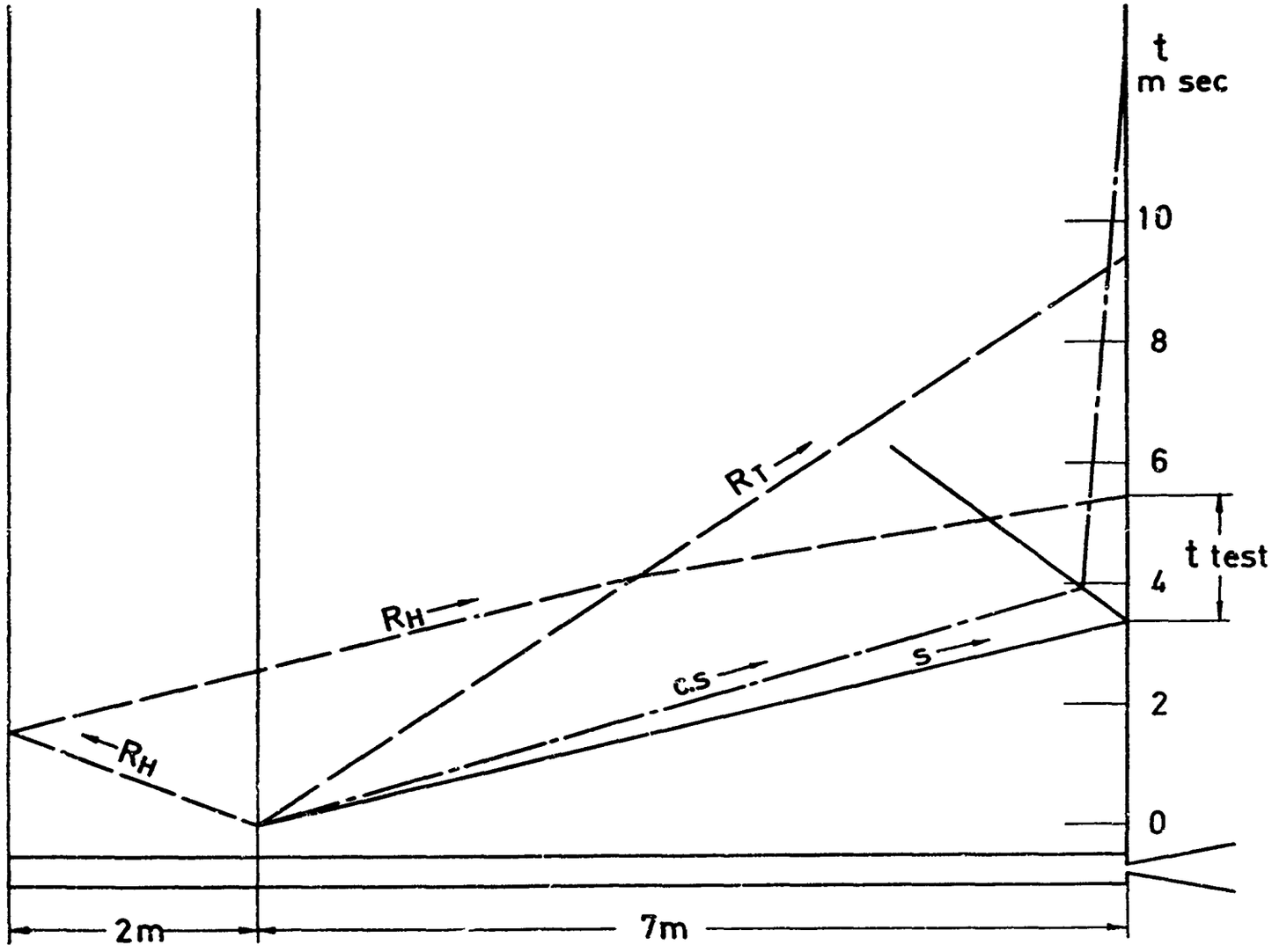

FIG. NO. 4: CALCULATED TIME EVENTS IN THE ACTUAL SHOCK TUBE.

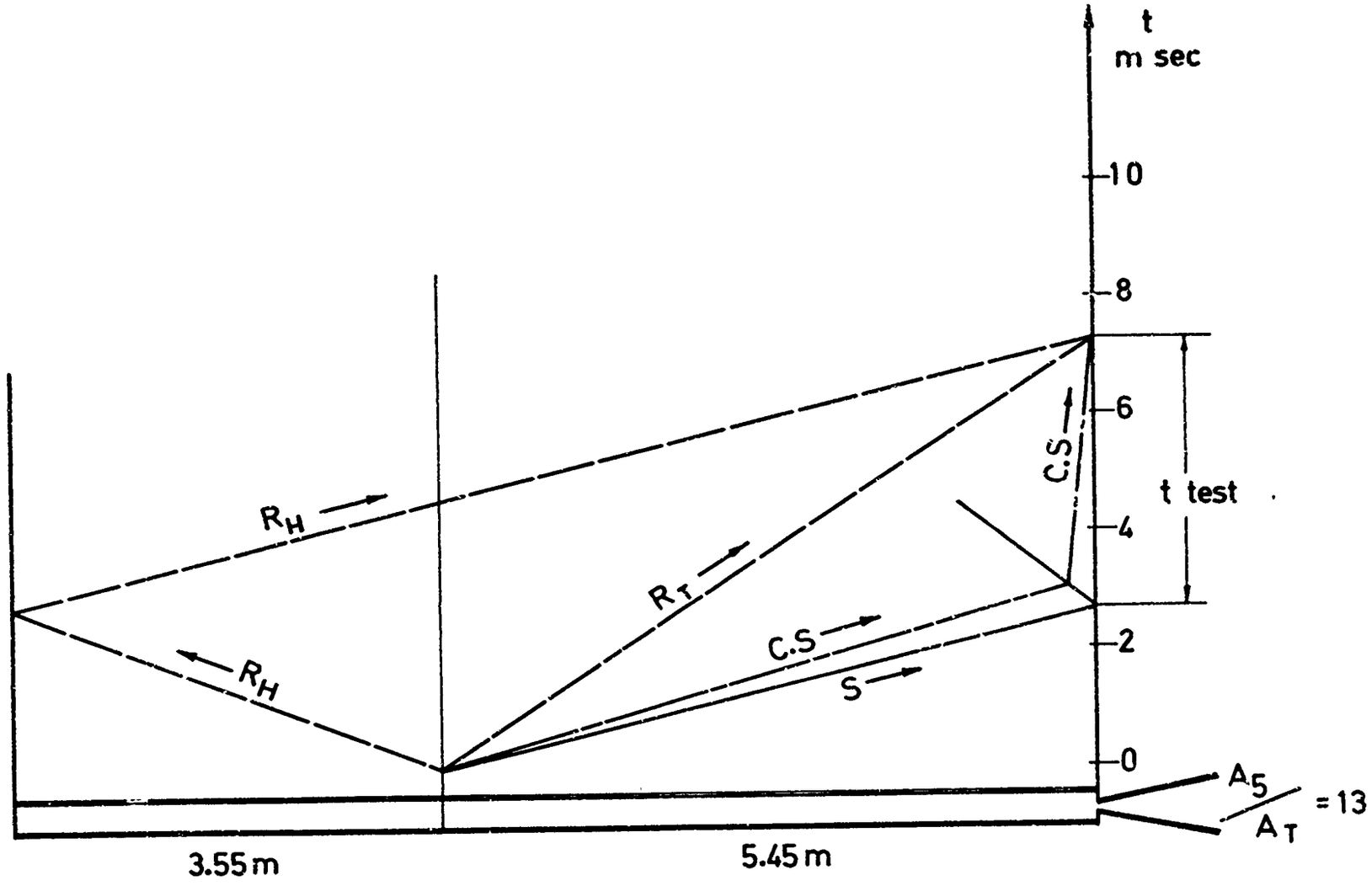

FIG. NO. 5: CALCULATED TIME EVENTS FOR MAXIMAL TEST DURATION SHOCK TUBE.

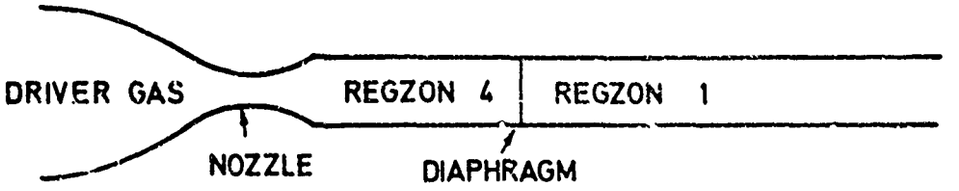

FIG. NO. 6: SHOCK TUBE WITH A NOZZLE IN THE DRIVER SECTION.

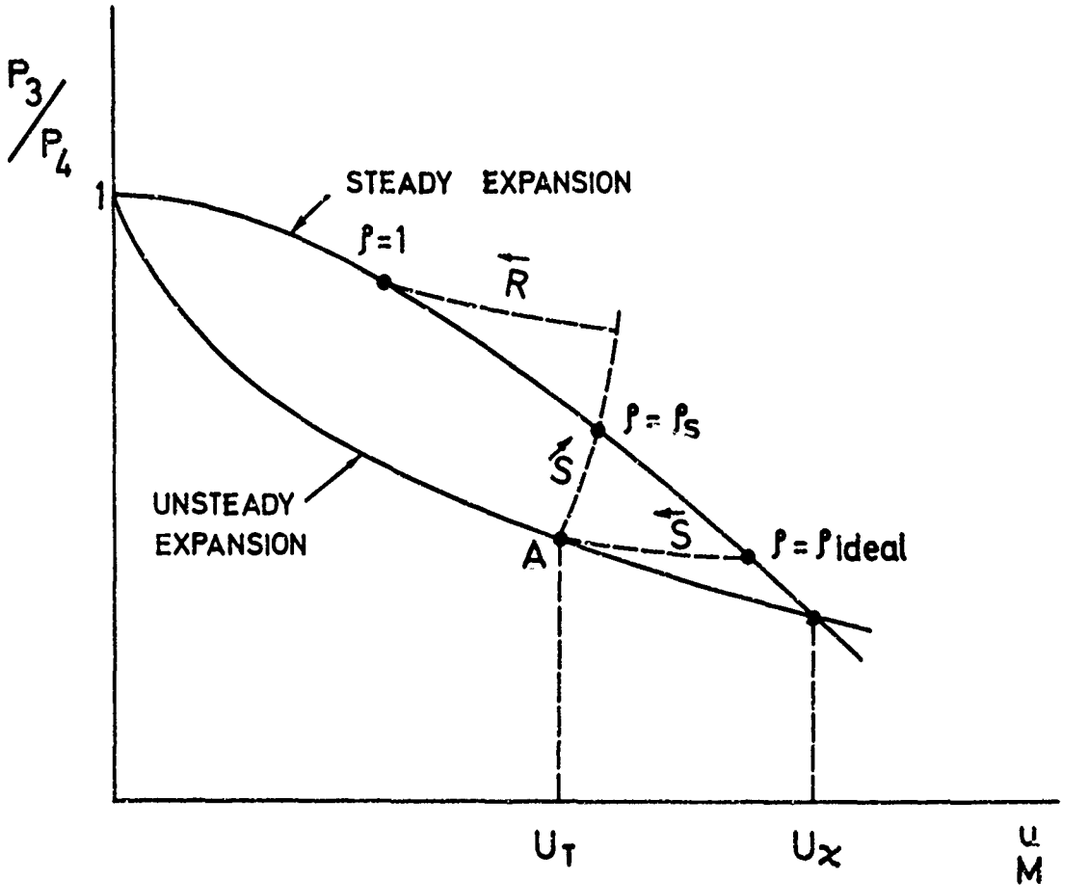

FIG. NO. 7: P-U DIAGRAM FOR SHOCK TUBE.

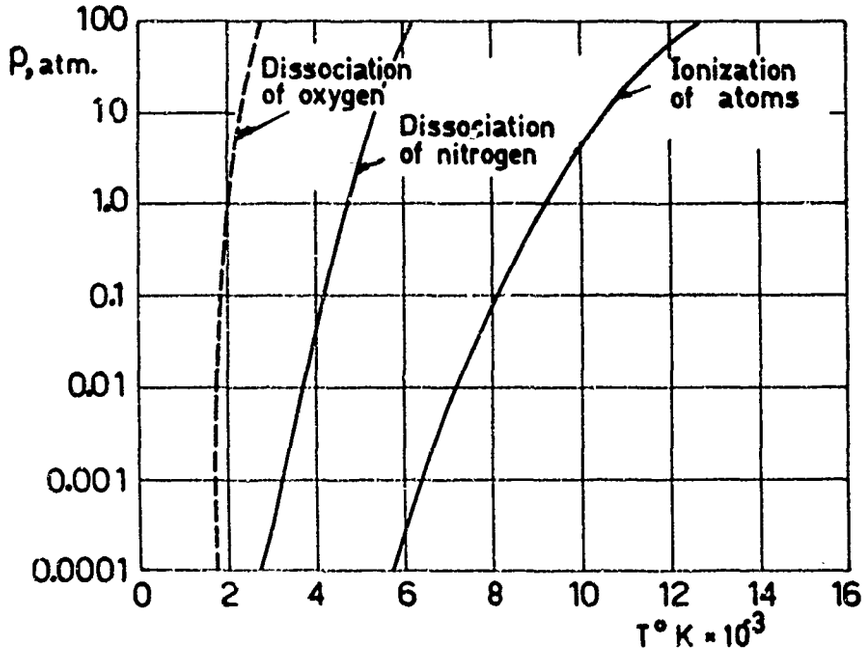

FIG. NO. 3: CHEMICAL REACTIONS EXISTING IN AIR.

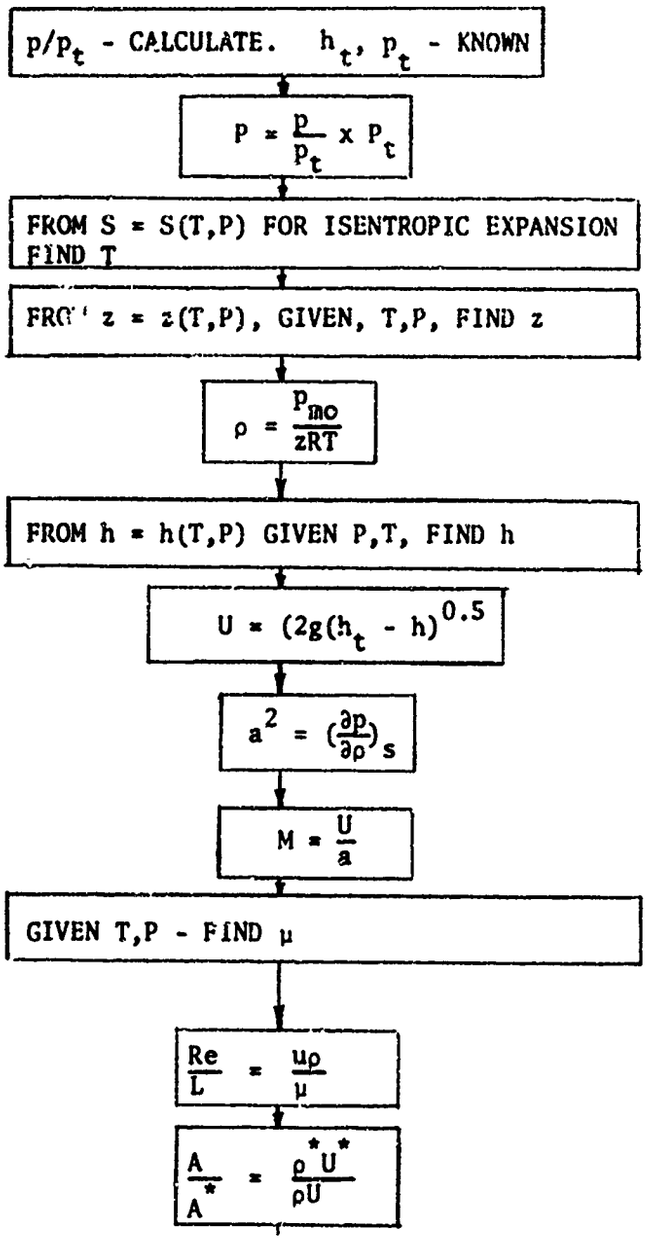

FIG. No. 9: FLOW SHART FOR CALCULATION OF FLOW IN THERMODYNAMIC EQUILIBRIUM

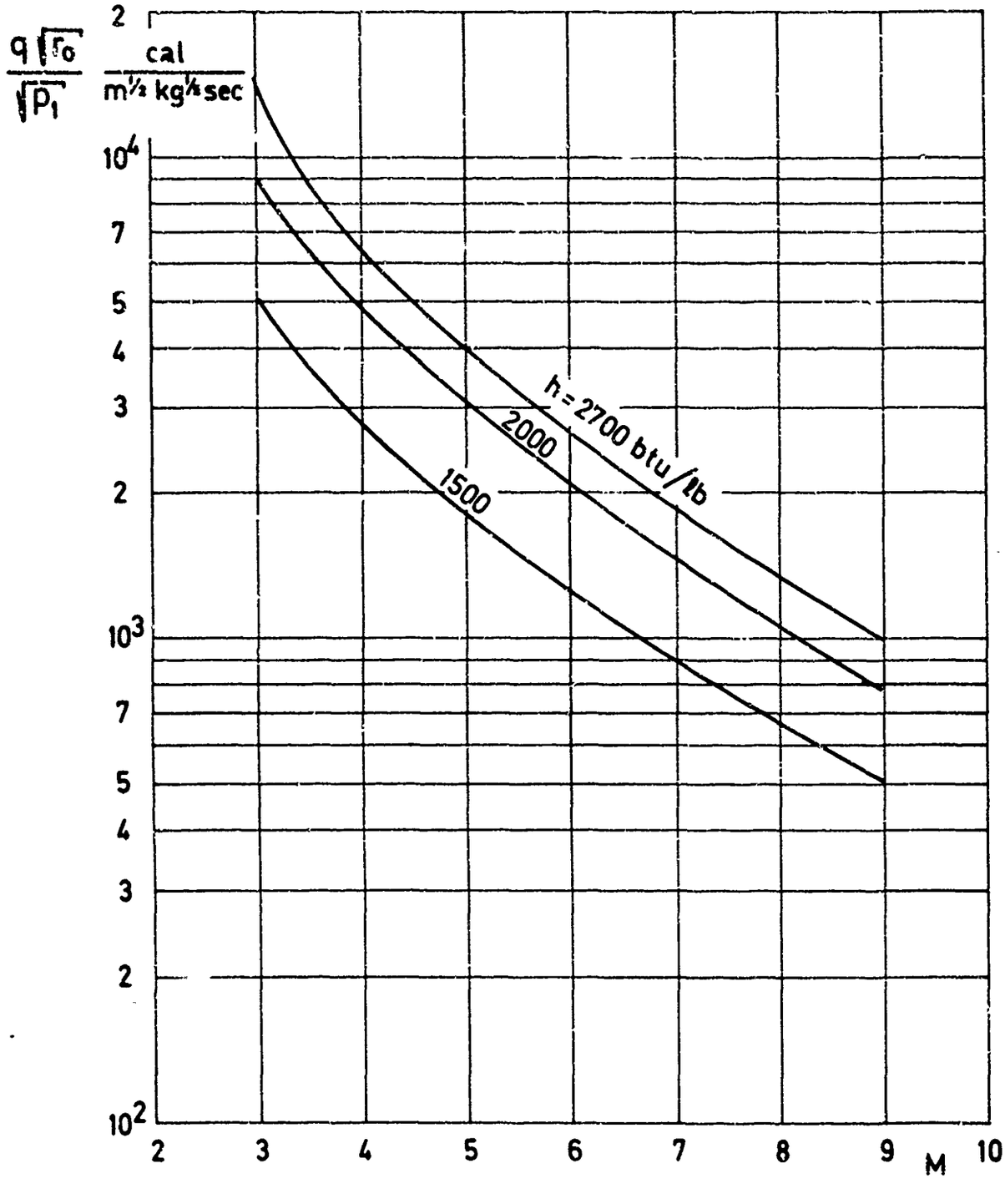

FIG. NO. 10: CALCULATED STAGNATION POINT HEAT TRANSFER RATE IN THE SUPERSONIC NOZZLE, VELOCITY DISTRIBUTION ACCORDING TO THE NEWTONIAN APPROXIMATION.

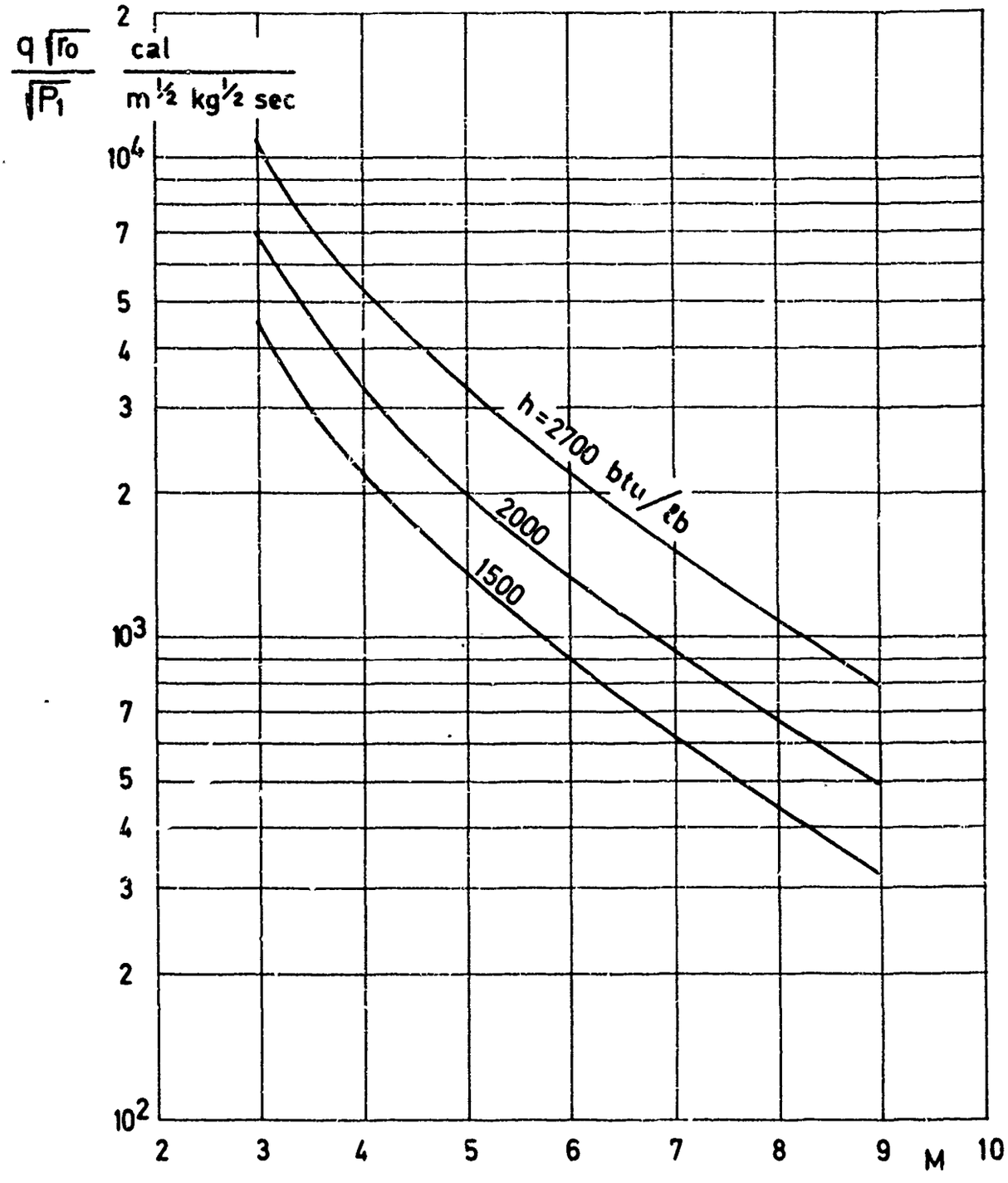

Fig. No. 10 A: CALCULATED STAGNATION POINT HEAT TRANSFER RATE IN THE SUPERSONIC NOZZLE, VELOCITY DISTRIBUTION ACCORDING TO THE POTENTIAL FLOW ON A SPHERE.

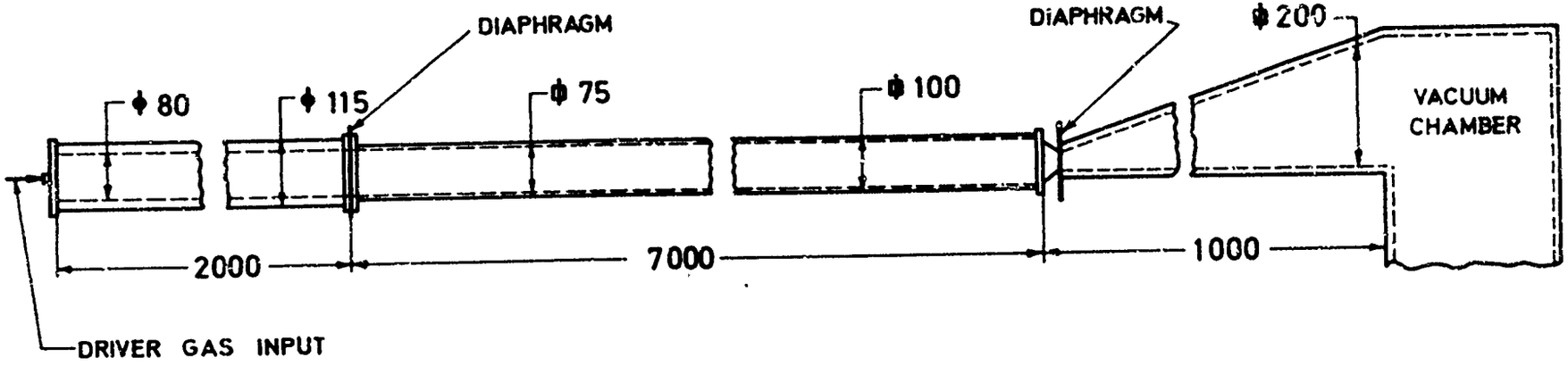

FIG. NO. 11 : MAIN PARTS OF THE SHOCK TUNNEL.

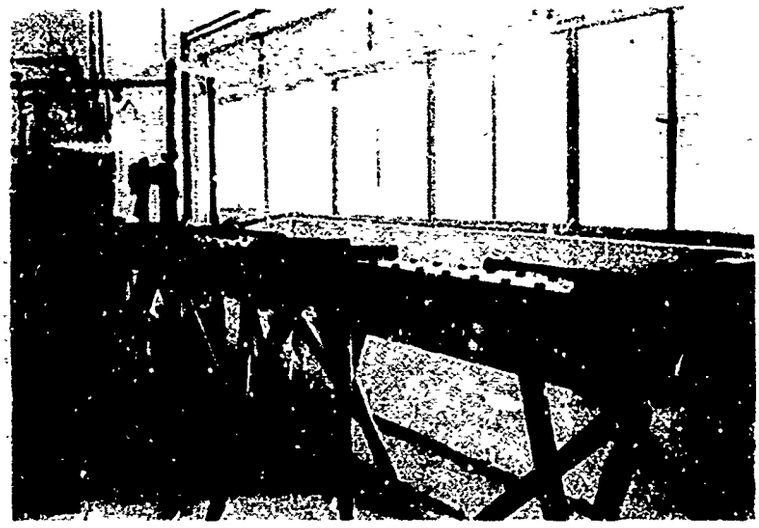

FIG. NO. 12: GENERAL VIEW OF THE SHOCK TUNNEL.

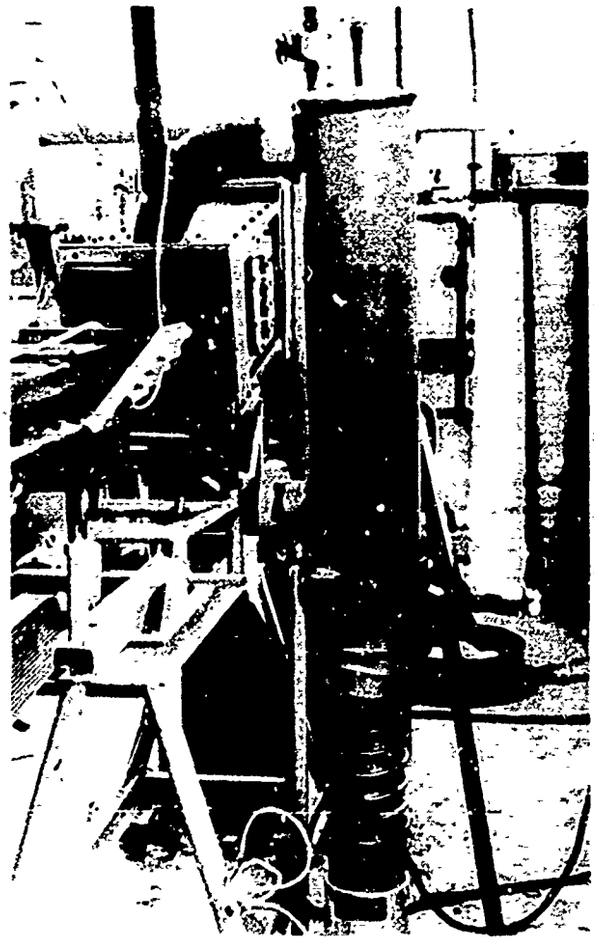

FIG. NO. 13: THE SUPERSONIC NOZZLE

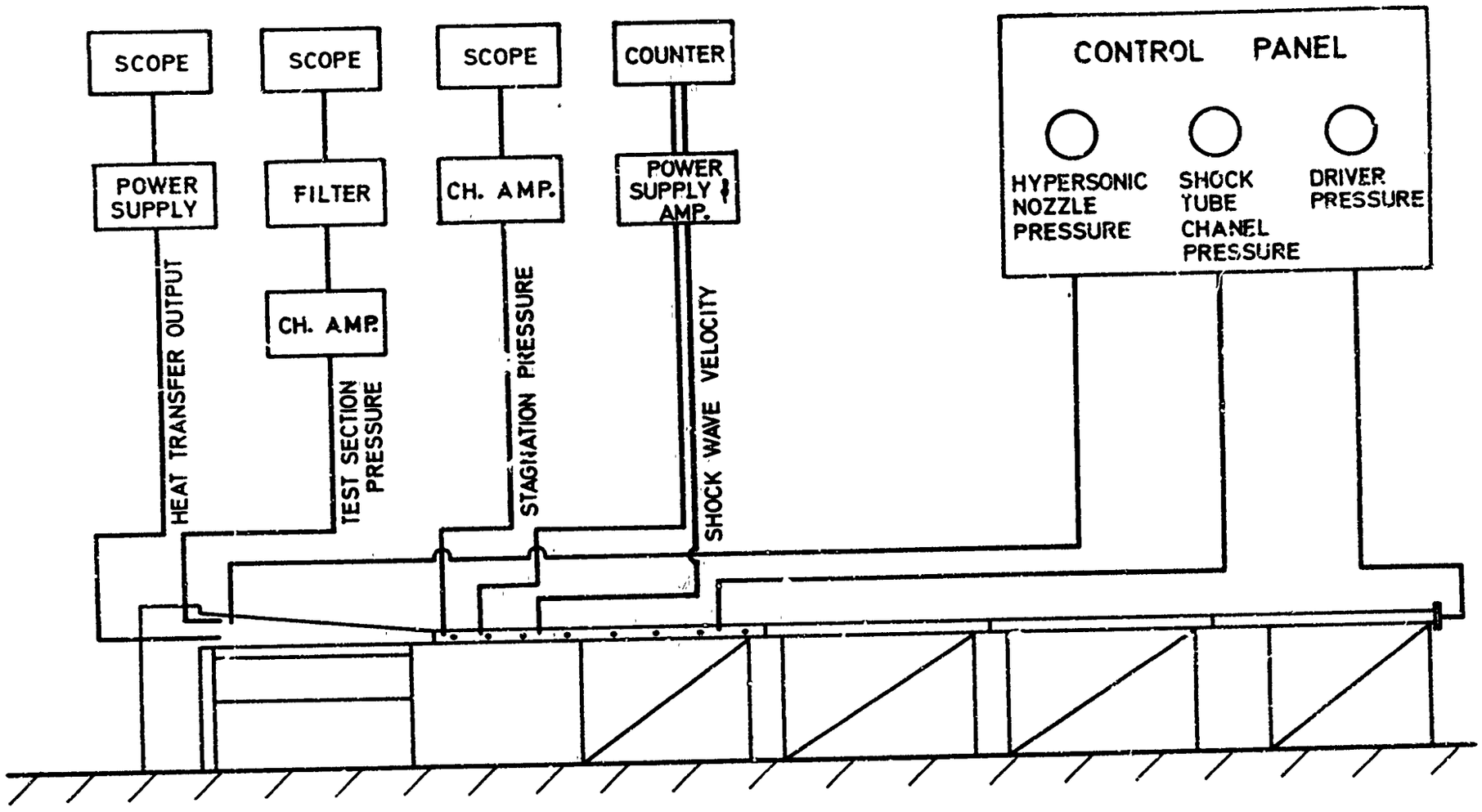

FIG NO. 14 : THE MEASURMENT SYSTEM.

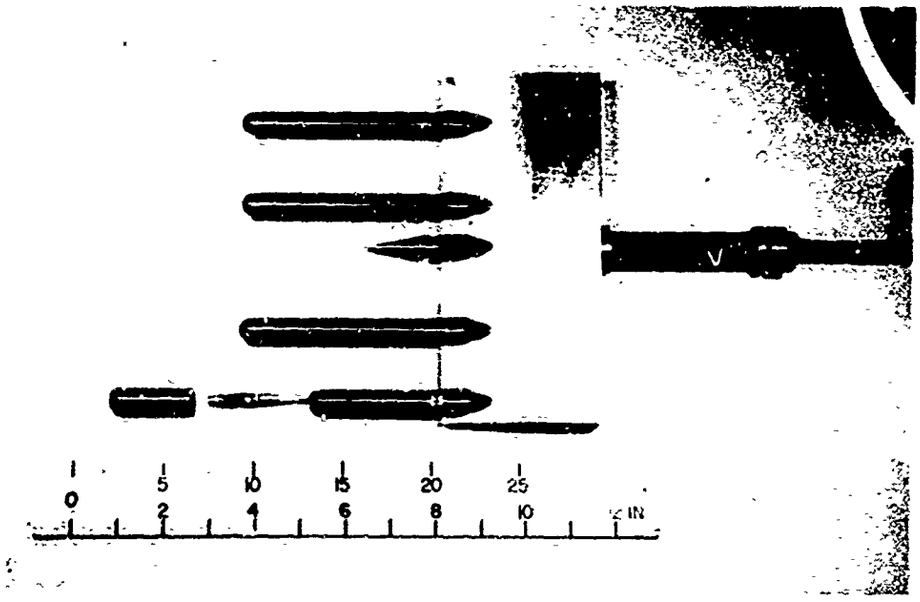

FIG. NO. 15: TOTAL PRESSURES RAKE.

FIG. NO. 16: TOTAL TEMPERATURE RAKE.

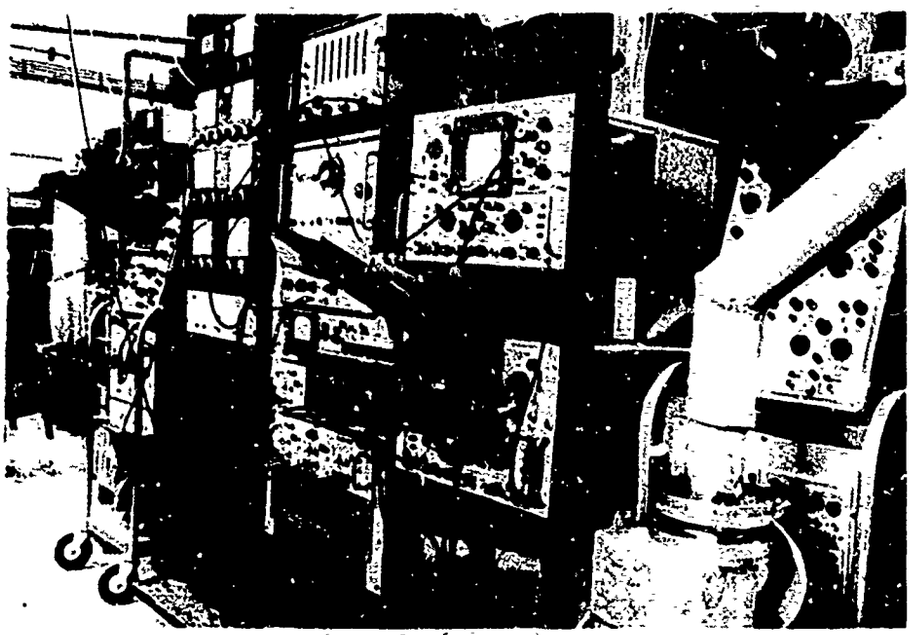

FIG. NO. 17: GENERAL VIEW OF ELECTRONIC EQUIPMENT.

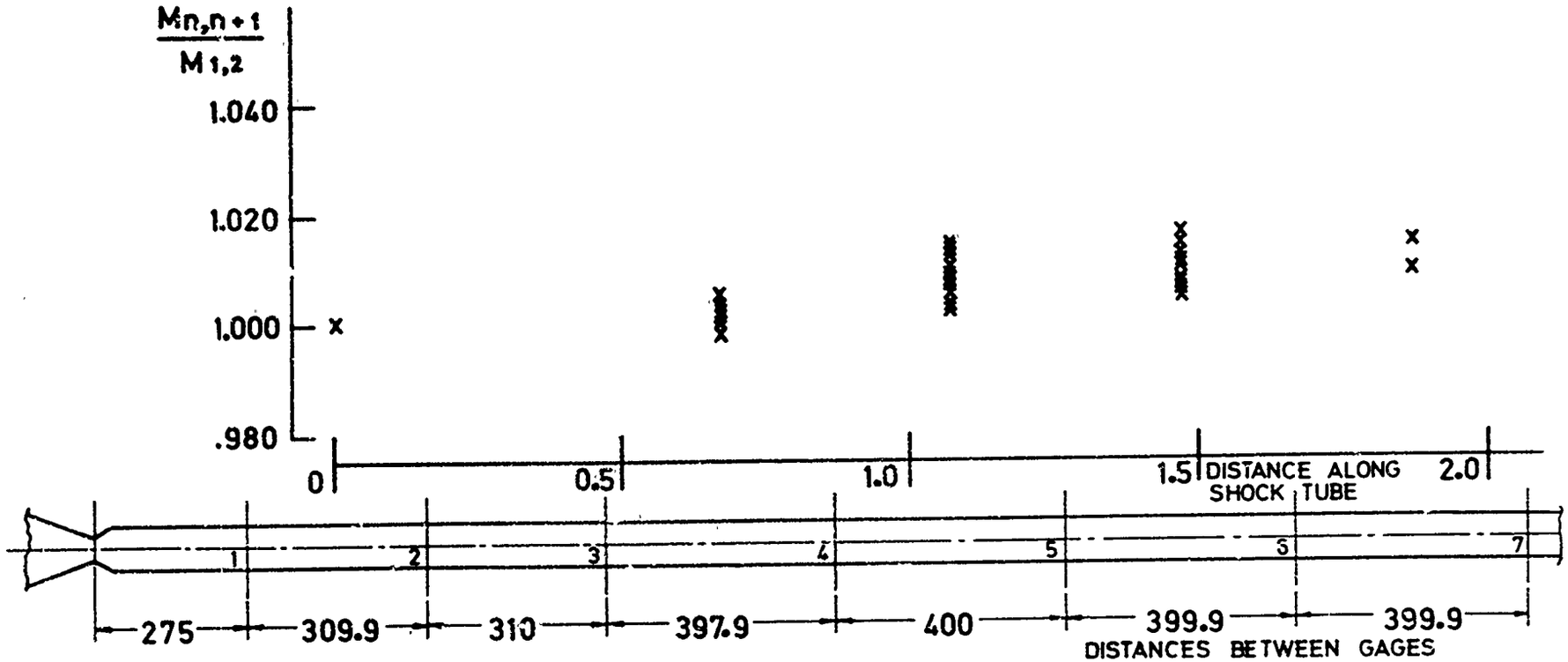

FIG. NO. 18: INCIDENT SHOCK WAVE ATTENUATION ALONG THE SHOCK TUBE.

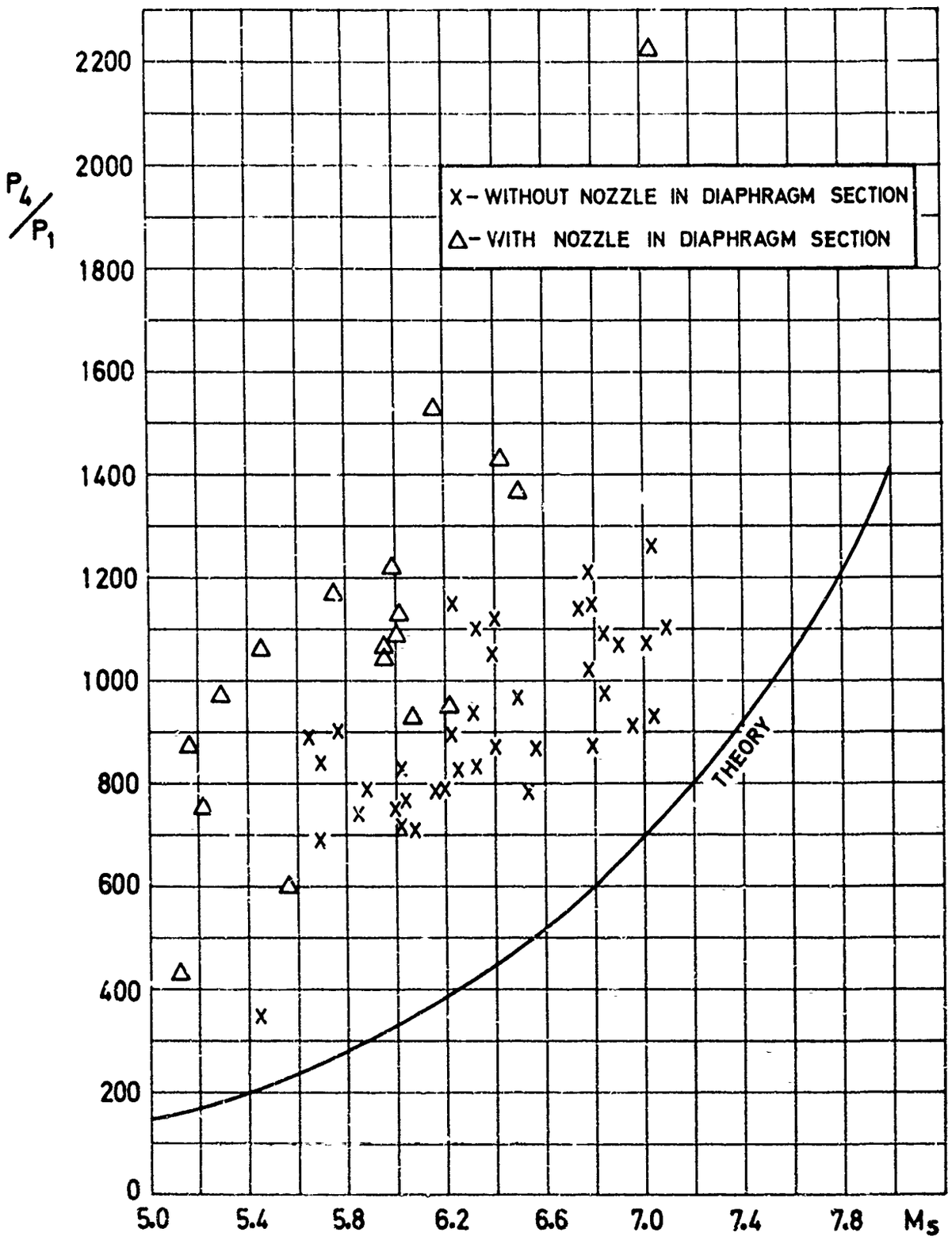

FIG. NO. 19: INITAL PRESSURES RATIO ACROSS THE SHOCK TUBE DIAPHRAGM FOR H_2/AIR AT ROOM TEMPERATURE.

HORIZONTAL SCALE 50 μ SEC/DIV

VERTICAL SCALE 100 PSI/DIV

$M_s = 6.2$

$P_1 = 38$ MM HG

FIG. NO. 22: TRACES OF PRESSURE MEASUREMENT AT THE END OF THE SHOCK TUBE.

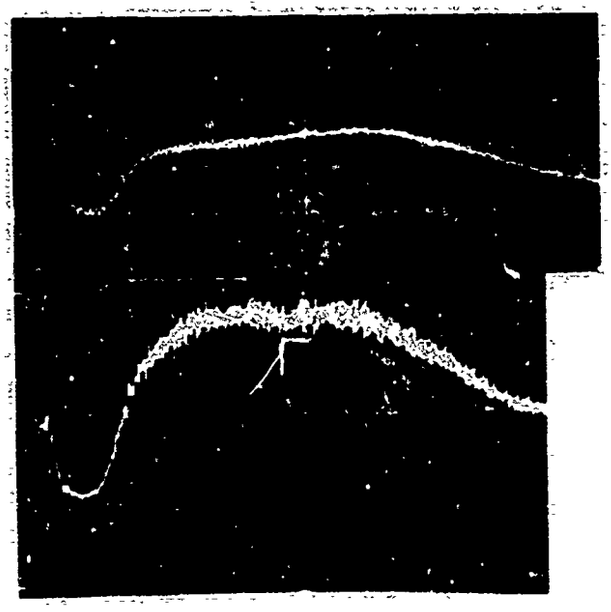

WITH NOZZLE

REGION 4

$M_s = 6.0$

$P_1 = 36$ MM HG

WITHOUT NOZZLE

REGION 4

$M_s = 5.9$

$P_1 = 38$ MM HG

HORIZONTAL SCALE 500 μ SEC/DIV.
VERTICAL SCALE 100 PSI/DIV.

FIG. NO. 23: TRACES OF PRESSURE MEASUREMENT AT THE END OF THE SHOCK TUBE.

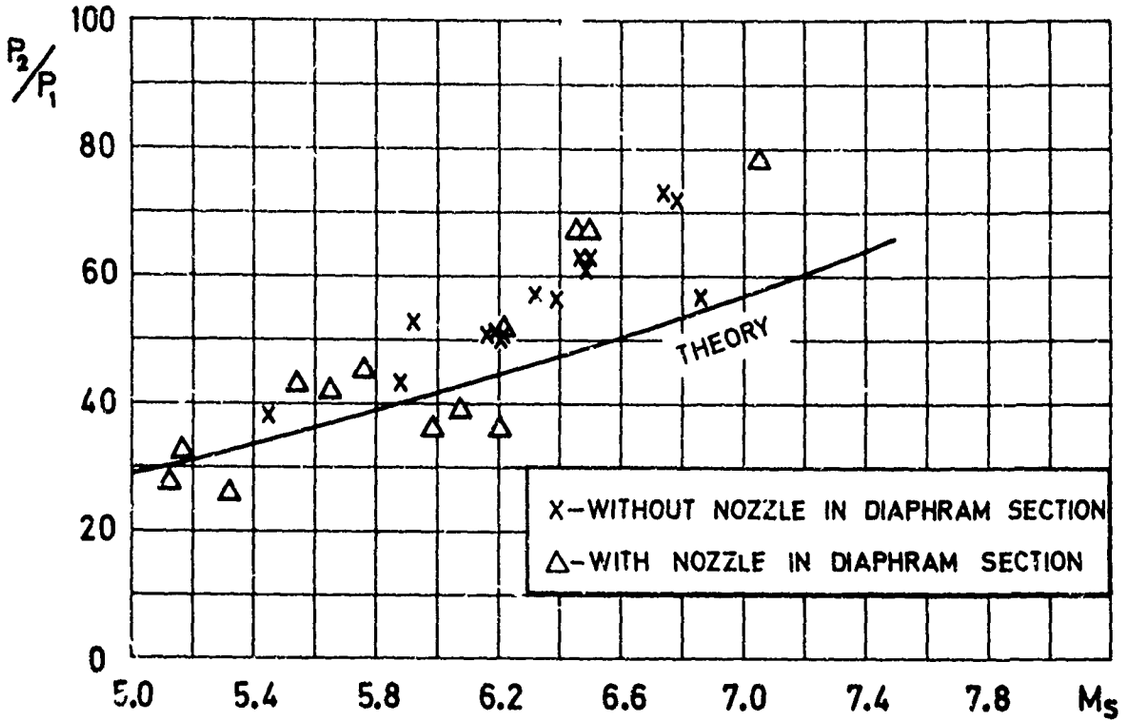

FIG. NO. 20: PRESSURE RATIO ACROSS INCIDENT SHOCK WAVE.

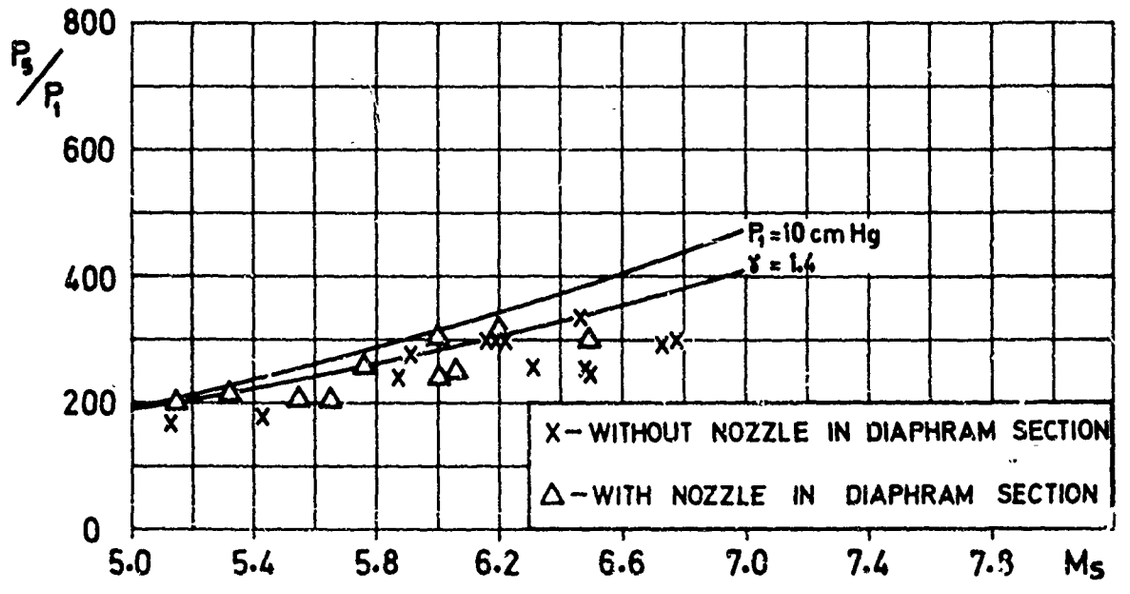

FIG. NO. 21: RATIO OF PRESSURE BEHIND THE REFLECTED SHOCK WAVE TO THE INITIAL PRESSURE IN THE SHOCK TUBE.

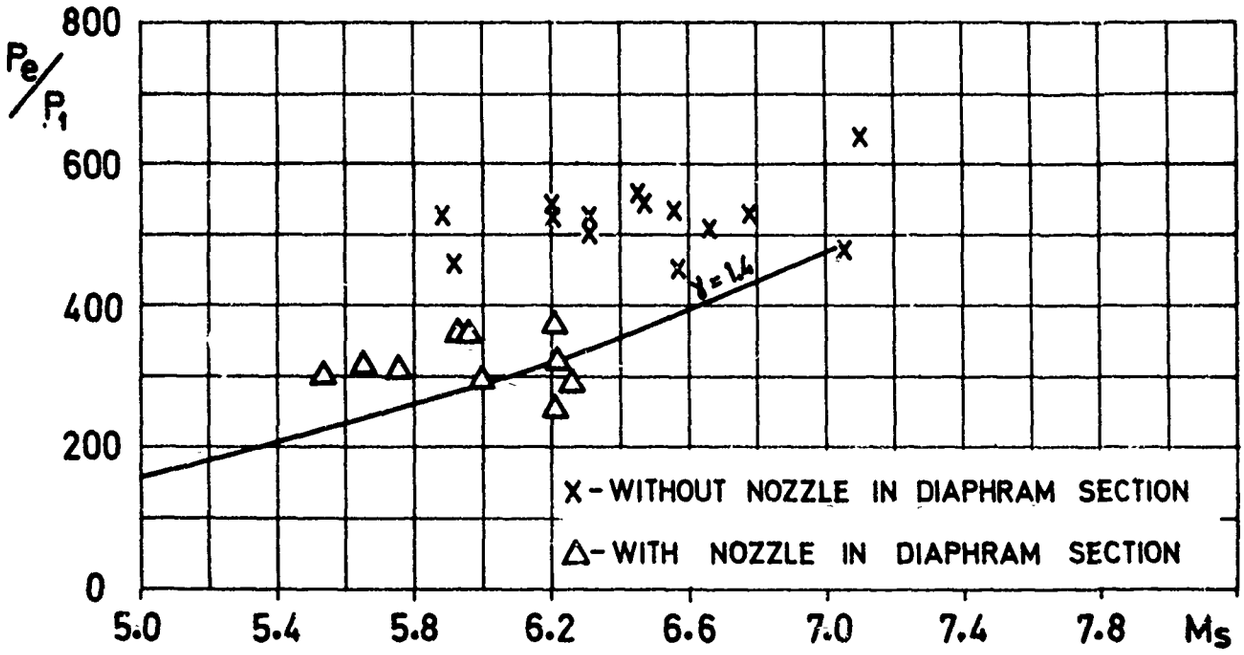

FIG. NO. 24: RATIO OF EQUILIBRIUM PRESSURE AT THE END OF THE SHOCK TUBE TO THE INITIAL PRESSURE IN THE SHOCK TUBE.

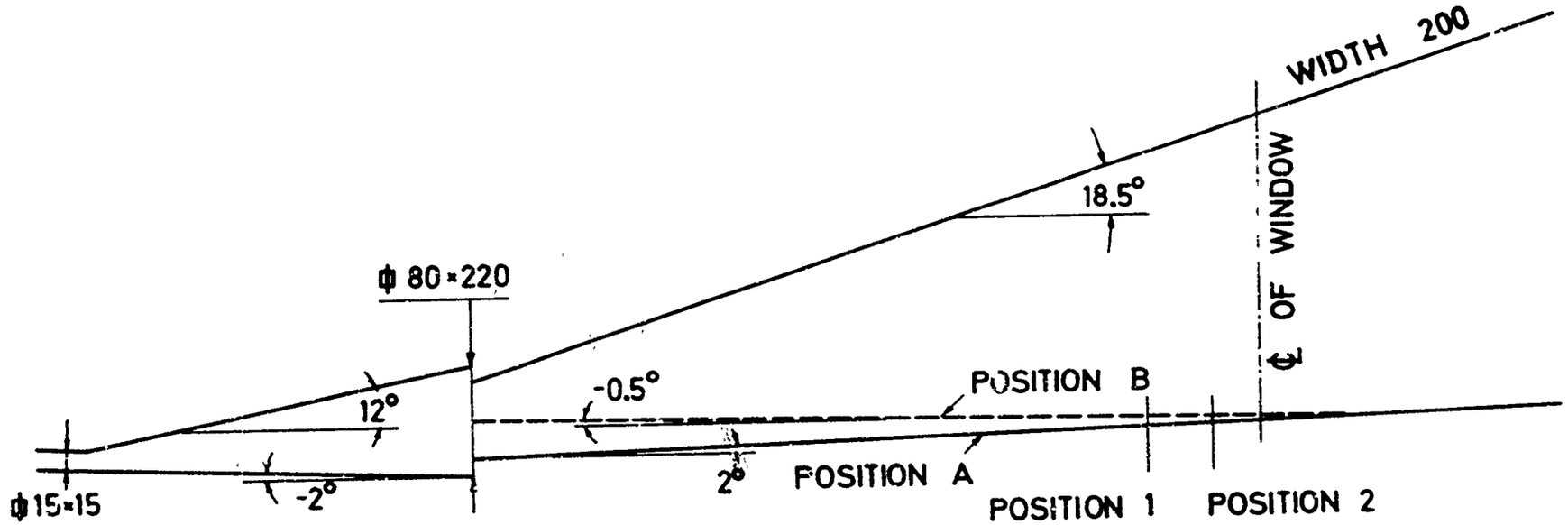

ALL DIMENSIONS IN MM.

FIG. NO. 25: THE SUPERSONIC NOZZLE.

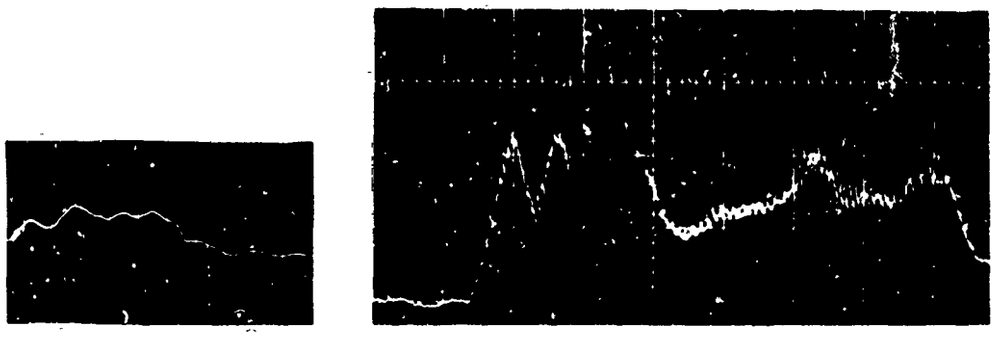

TOTAL PRESSURE BEHIND THE SHOCK WAVE

VERTICAL SCALE 4 PSI/DIV.

HORIZONTAL SCALE 500 μ SEC/DIV.

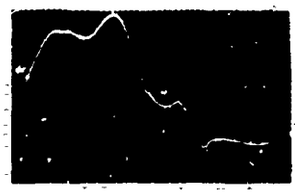

STATIC PRESSURE

VERTICAL SCALE 0.02 PSI/DIV.

HORIZONTAL SCALE 500 μ SEC/DIV.

FIG. NO. 26: PRESSURE GAUGE TRACES IN TEST SECTION.

NOZZLE IN POSITION A

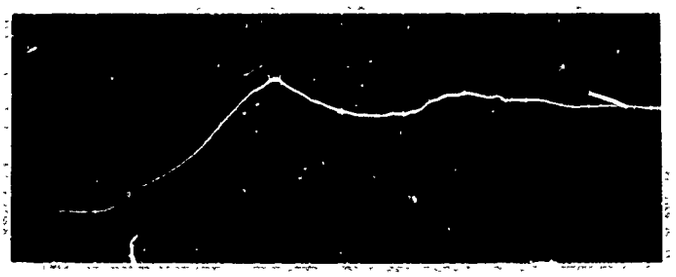

NOZZLE IN POSITION B

FIG. NO. 27: HEAT TRANSFER RATE MEASUREMENTS TRACES IN TEST SECTION.

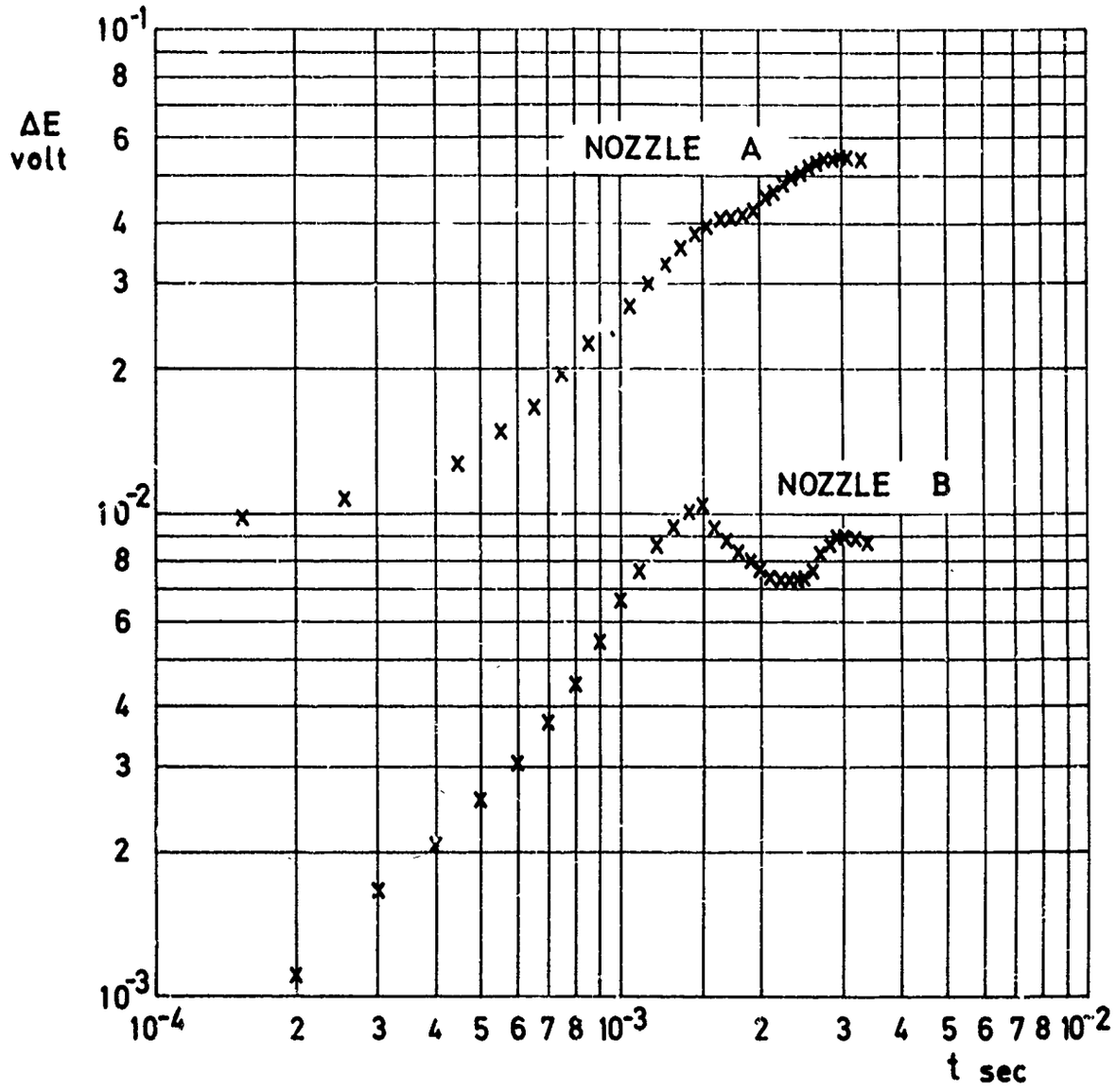

FIG. NO. 28: ΔV VS. T FROM HEAT TRANSFER RATE MEASURMENT.

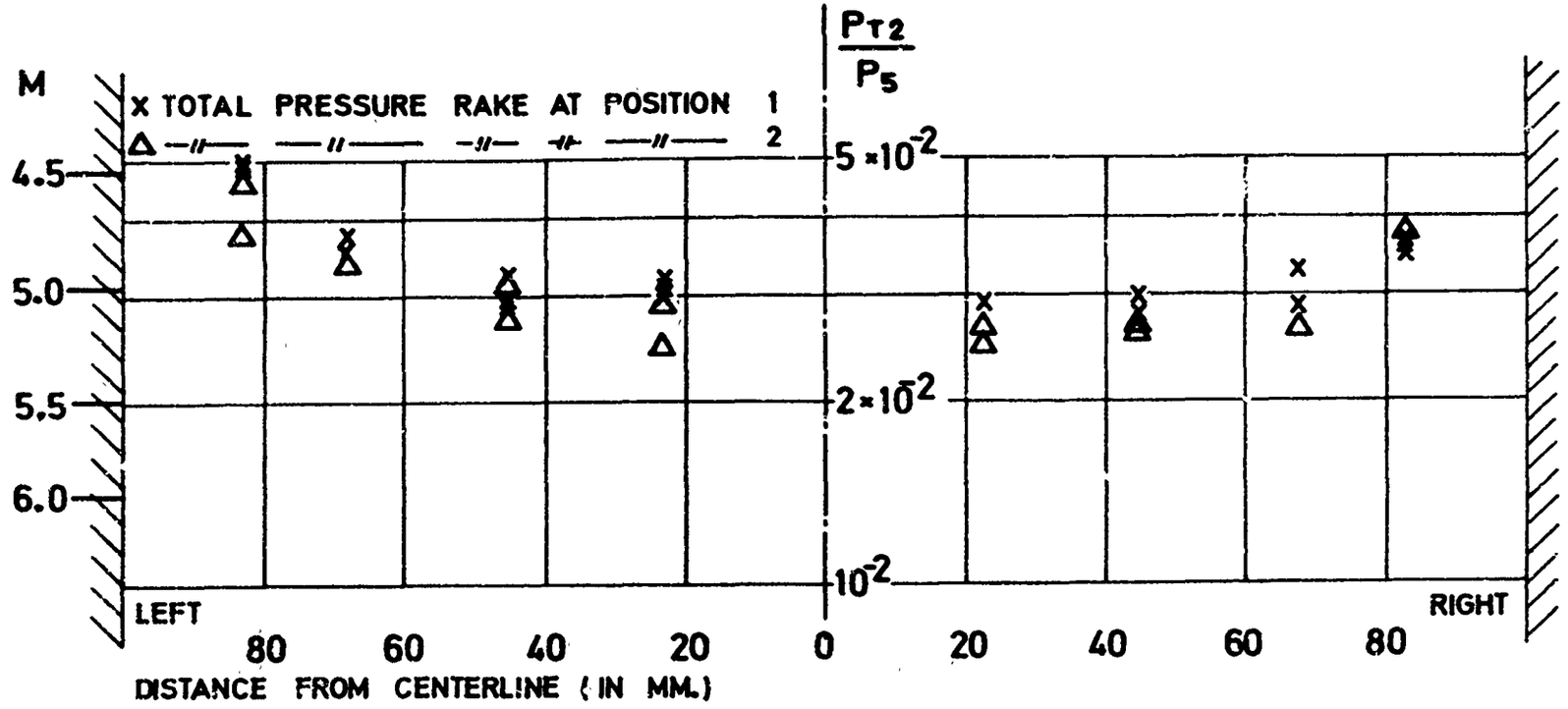

FIG. NO. 29: TOTAL PRESSURES BEHIND A SHOCK WAVE, HORIZONTAL DISTRIBUTION. NOZZLE IN POSITION A.

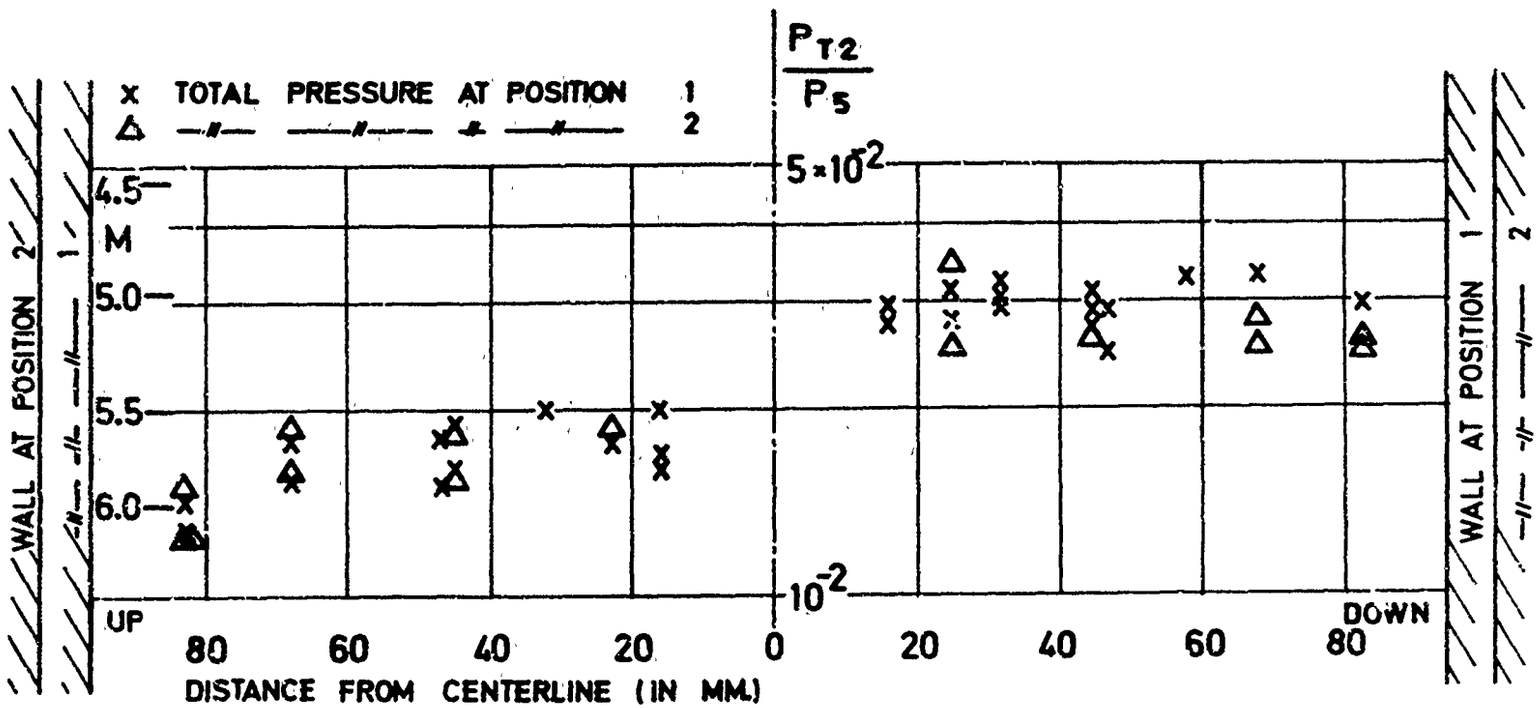

FIG. NO. 30: TOTAL PRESSURES BEHIND A SHOCK WAVE, VERTICAL DISTRIBUTION. NOZZLE IN POSITION A.

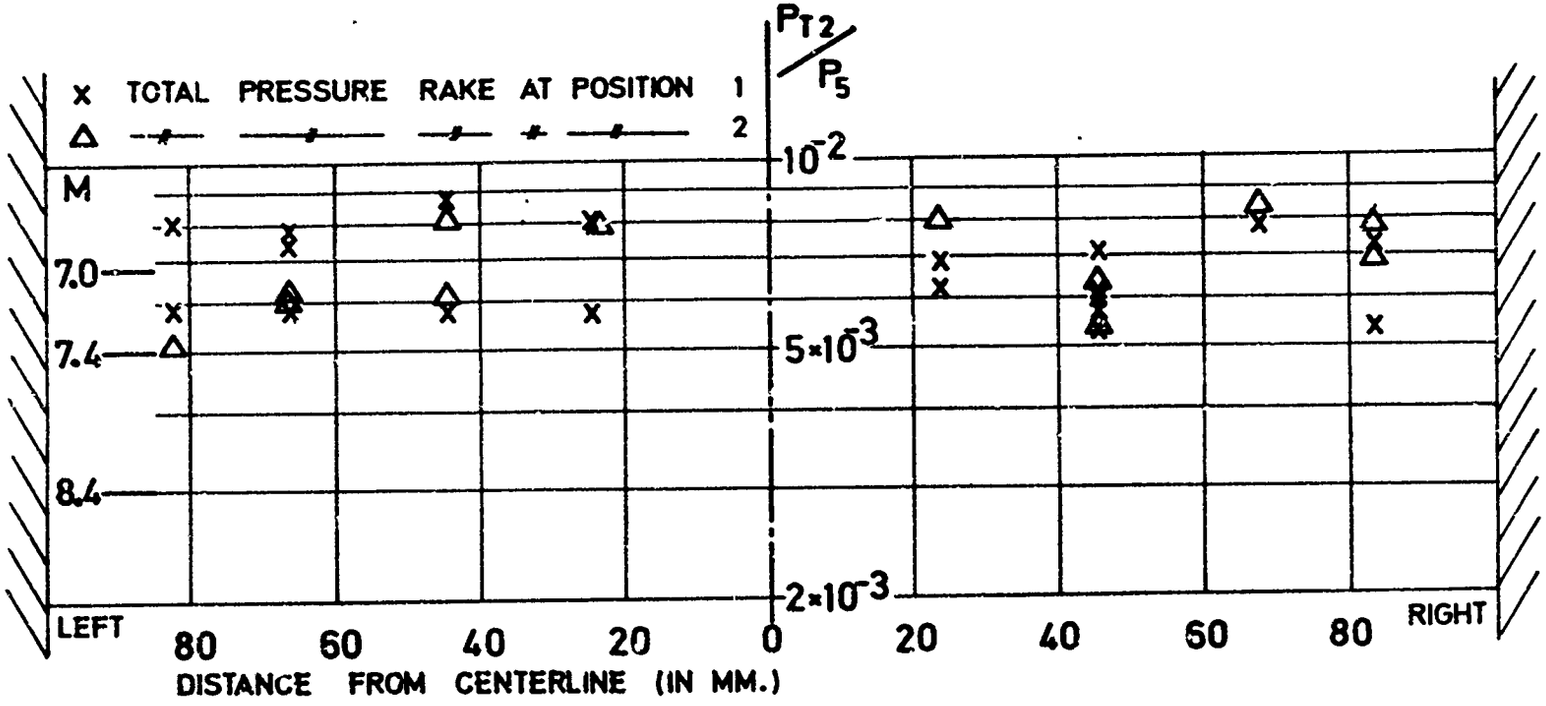

FIG. NO. 31: TOTAL PRESSURES BEHIND A SHOCK WAVE, HORIZONTAL DISTRIBUTION. NOZZLE IN POSITION 8.

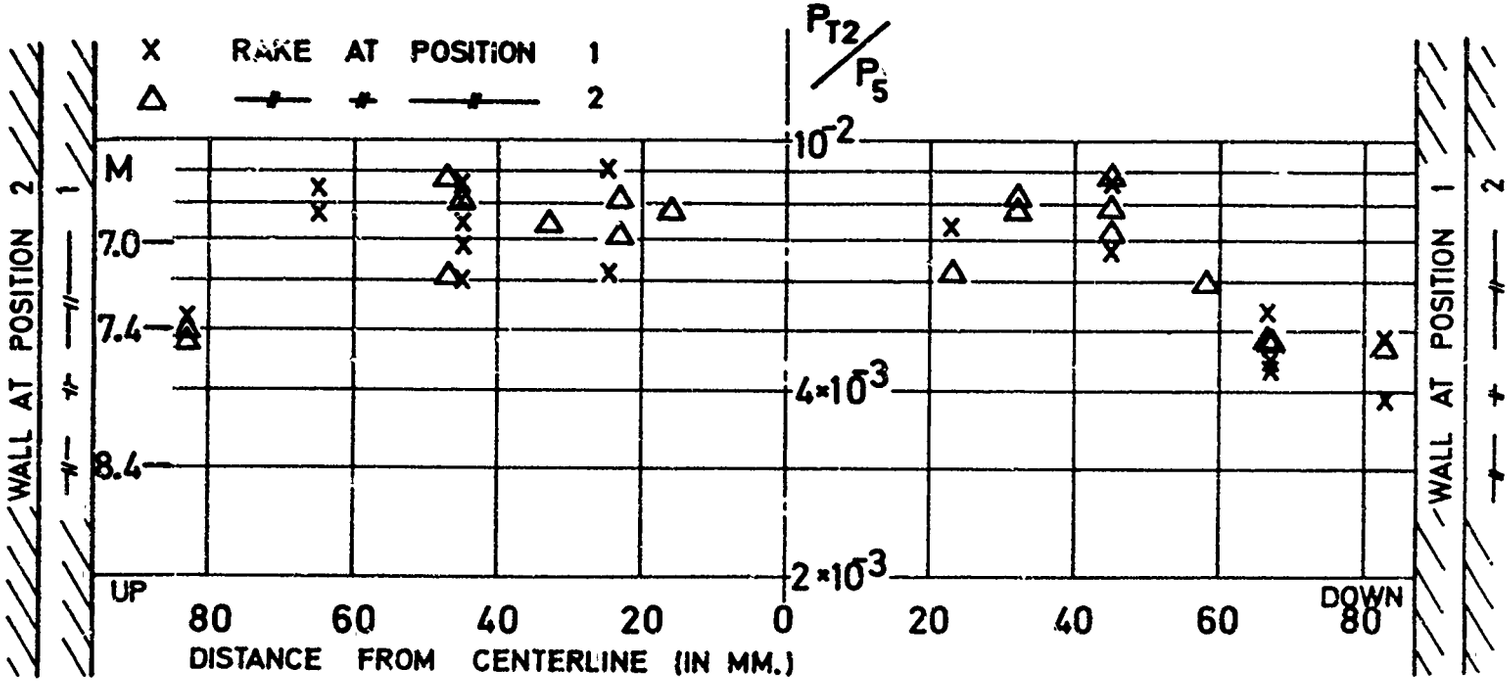

FIG. NO. 32: TOTAL PRESSURES BEHIND A SHOCK WAVE, VERTICAL DISTRIBUTION. NOZZLE IN POSITION B .

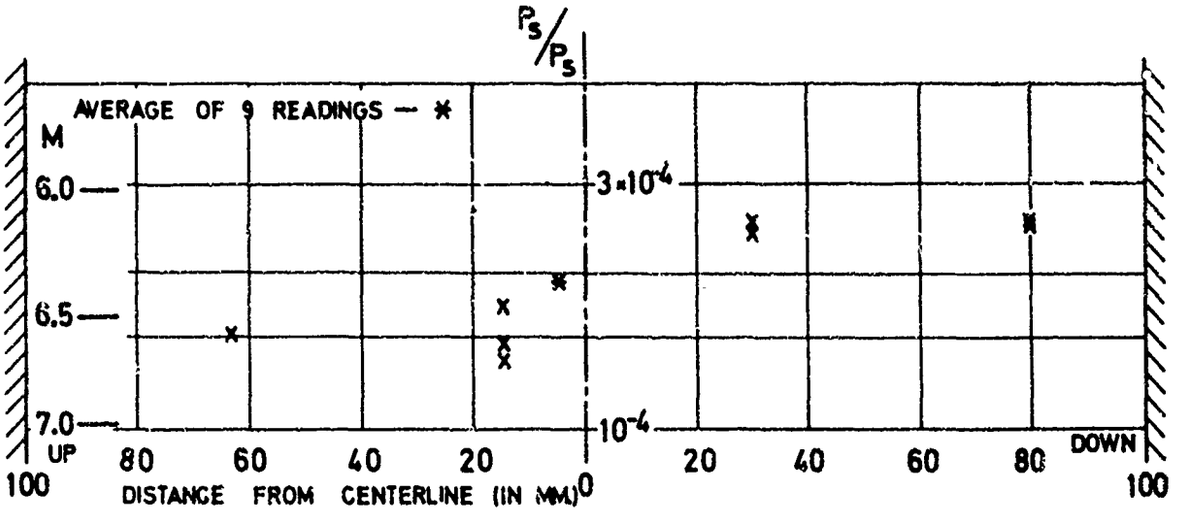

FIG. NO. 33: VERTICAL DISTRIBUTION OF STATIC PRESSURES. NOZZLE IN POSITION A.

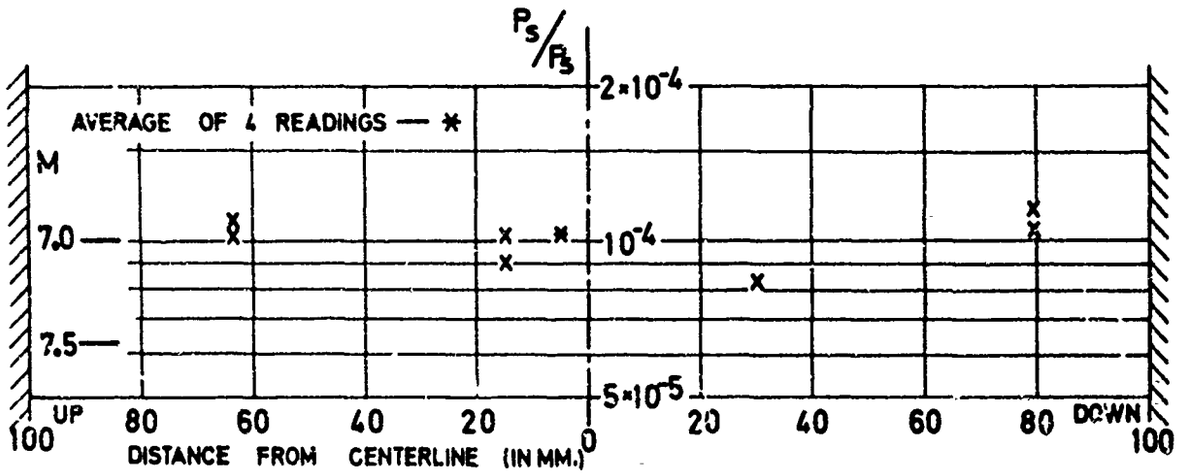

FIG. NO. 34: VERTICAL DISTRIBUTION OF STATIC PRESSURES. NOZZLE IN POSITION B.

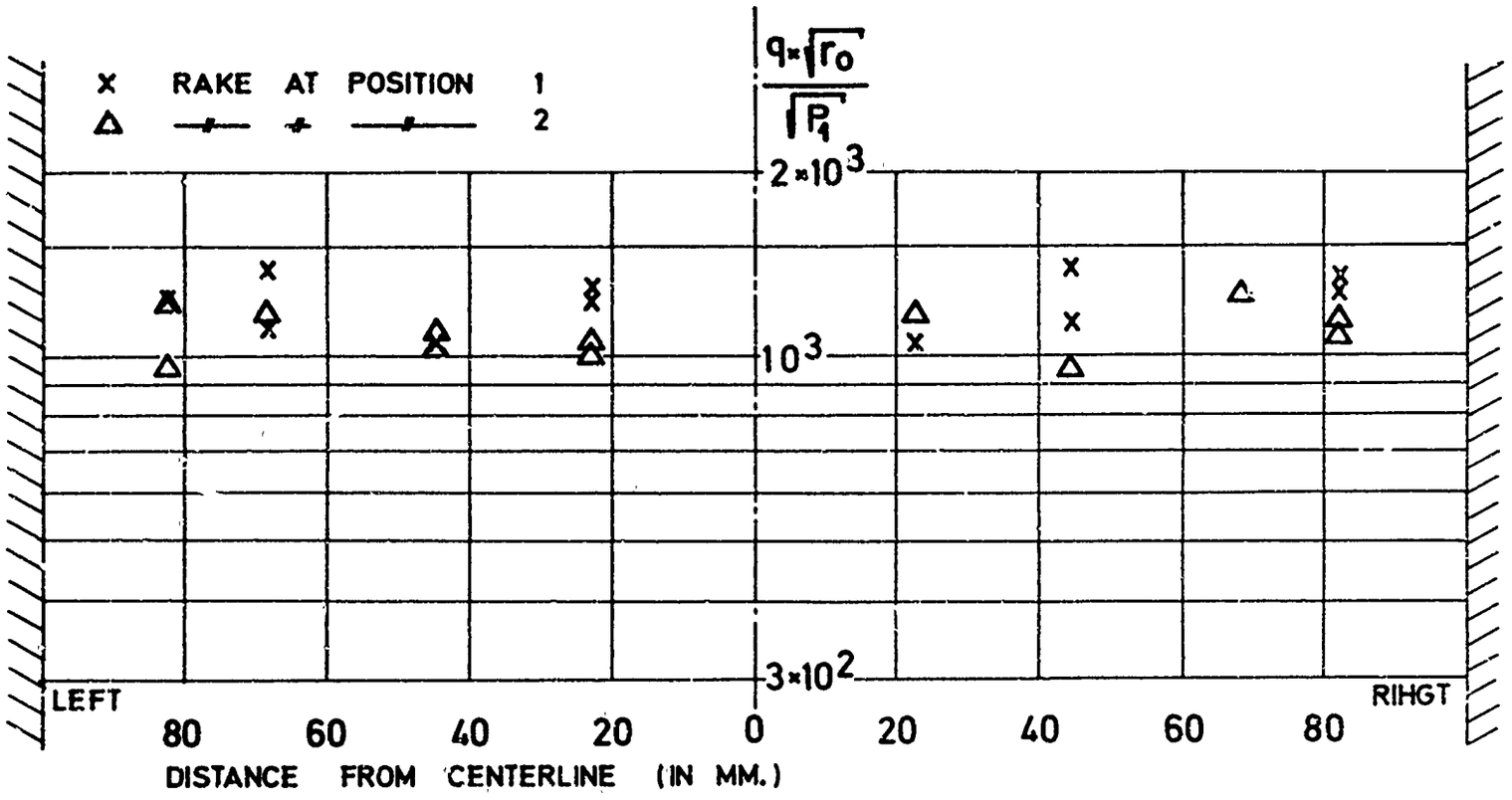

FIG. NO. 35: HORIZONTAL DISTRIBUTION OF STAGNATION POINT HEAT TRANSFER RATES. NOZZLE IN POSITION A.

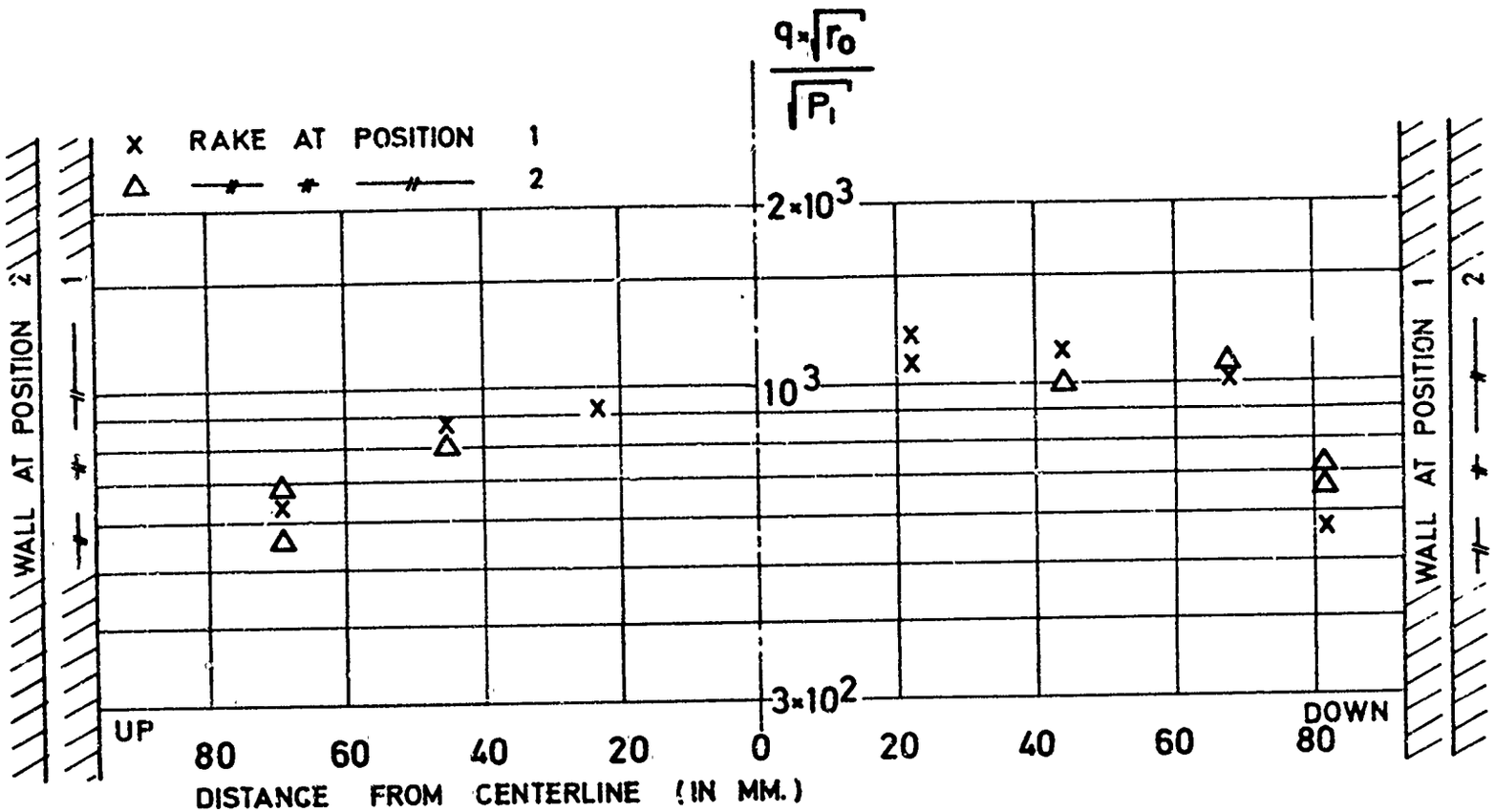

FIG. NO. 36: VERTICAL DISTRIBUTION OF STAGNATION POINT HEAT TRANSFER RATES. NOZZLE IN POSITION A.

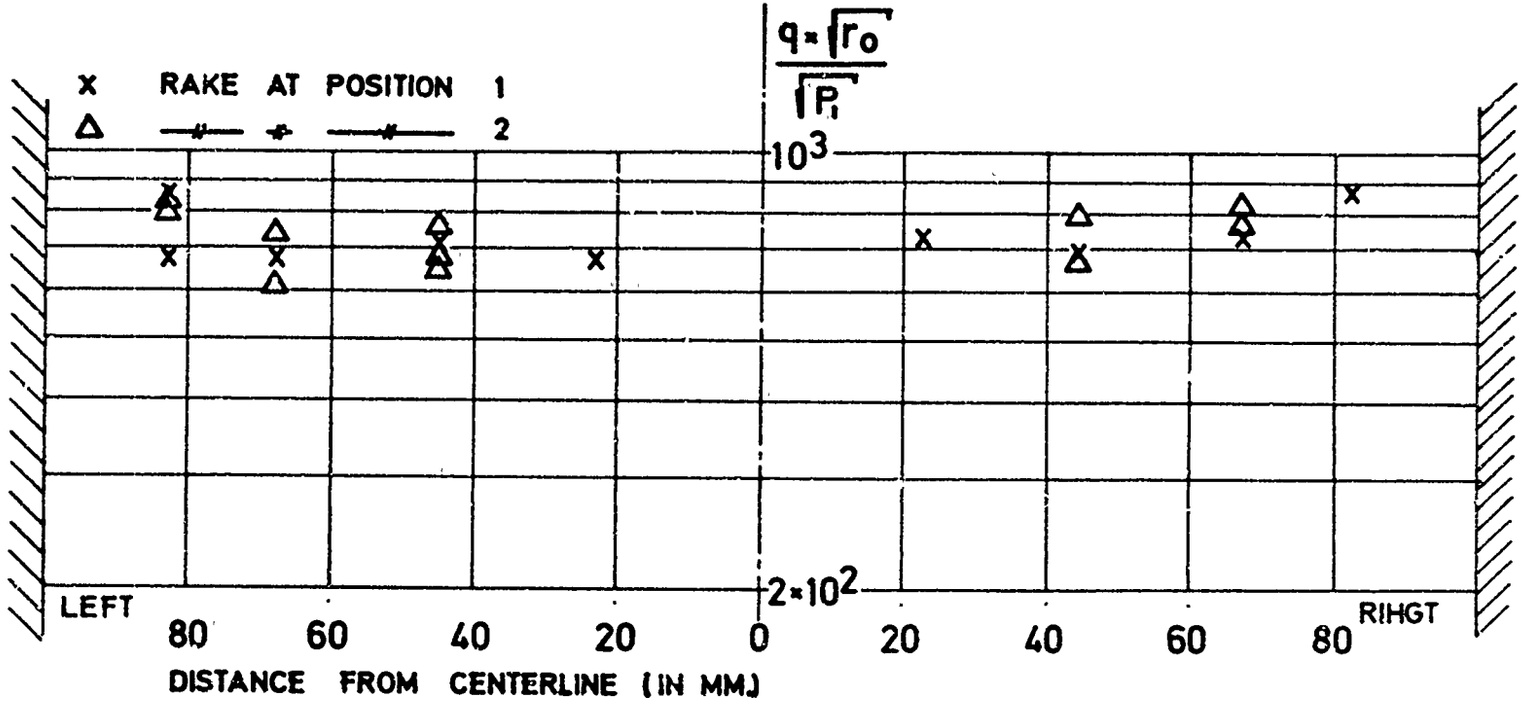

FIG. NO. 37: HORIZONTAL DISTRIBUTION OF STAGNATION POINT HEAT TRANSFER RATES NOZZLE IN POSITION 3.

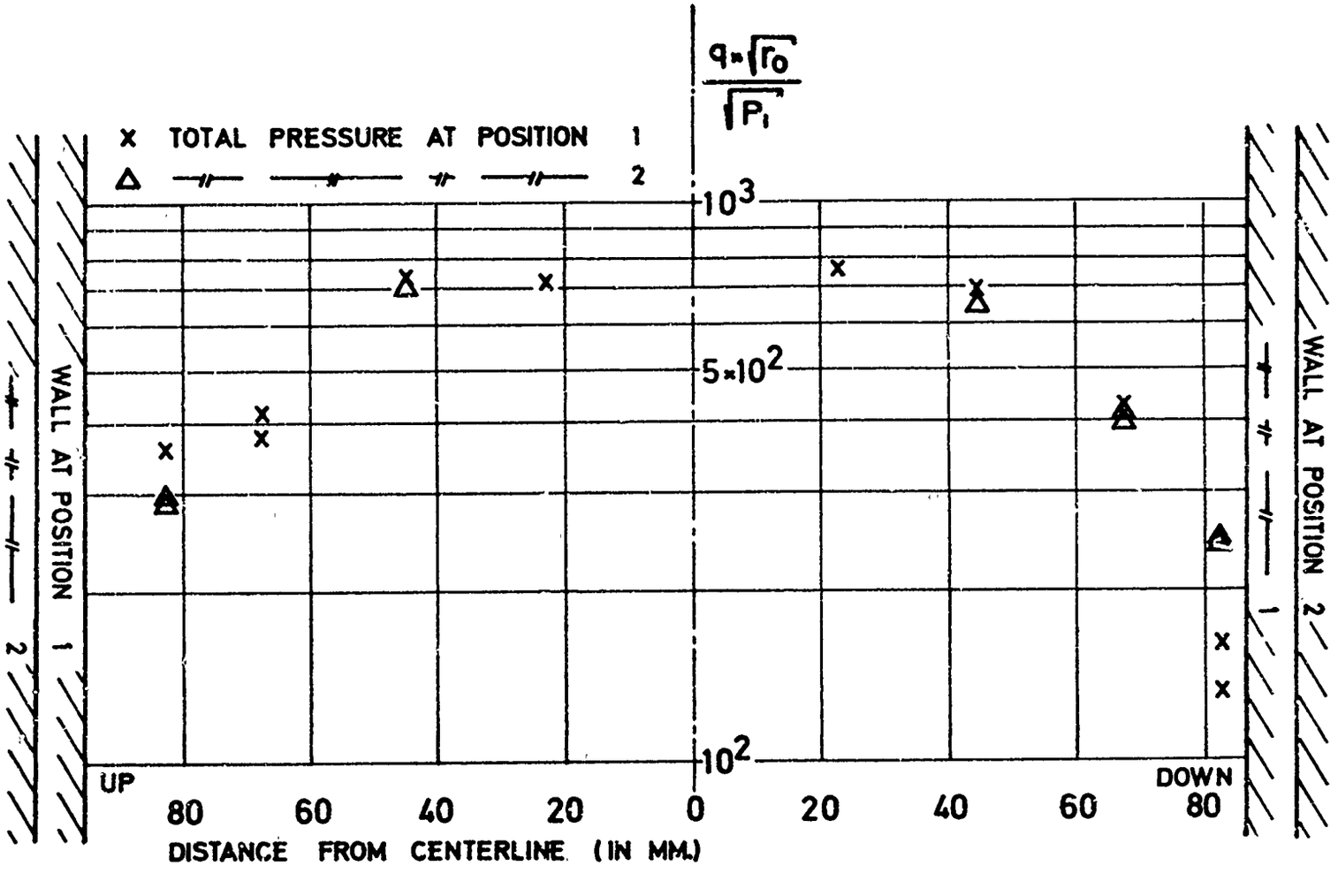

FIG. NO. 38: VERTICAL DISTRIBUTION OF STAGNATION POINT HEAT TRANSFER RATES. NOZZLE IN POSITION B.